Title: Unequal genetic redundancy among the rice transcription factors OsMADS2 and OsMADS4 reveals distinct roles in floret organ development

Short Title: Mechanistic framework for unequal genetic redundancy among rice *PISTILLATA* paralogs

Authors:

Mohamed ZamZam[1] Sharad Singh[1], Raghavaram Peesapati[1], Sandhan Prakash[1], Sara Simonini[2] , Ueli Grossniklaus[2] and Usha Vijayraghavan*[1]

[1] Department of Microbiology and Cell Biology, Indian Institute of Science, Bangalore 560012, India
[2] Institute of Plant and Microbial Biology, University of Zurich, Zollikerstrasse 107, CH8008, Zurich, Switzerland

***Corresponding author:** Usha Vijayraghavan

Department of Microbiology and Cell Biology,

Indian Institute of Science, Bangalore 560012, India

Email: uvr@iisc.ac.in and uvr123@gmail.com

Tel.: +918023600168 14 Fax: +918023602697

Abstract:

Functional diversification of transcription factors and of their downstream targets contributes to the emergence of new organ morphologies. To better understand the molecular mechanisms underlying floral organ specification in rice, we investigated the function of *OsMADS2* and *OsMADS4*, the rice *PISTILLATA* (*PI*) paralogs controlling lodicule and stamen formation. The morphological characterization of *osmads2* null mutants generated by CRISPR/Cas9 reiterated OsMADS2's nonredundant role in lodicule development. Furthermore, it uncovered unreported roles in controlling flowering time, floral meristem size, floral organ number, cell wall metabolism, and sterile lemma development. Although downregulation of *OsMADS4* did not affect floral organ development, doubly perturbed *osmads2*$^{d8/d8}$ *osmads4kd* florets exhibited more severe abnormalities than the *osmads2* single mutant. Doubly perturbed inflorescences also exhibited defective rachis extension and parthenocarpy. Remarkably, ubiquitous overexpression of *OsMADS4* in *osmads2* rescued the different abnormalities of the *osmads2* mutant but resulted in defective anther development and reduced seed set, phenotypes also observed when *Arabidopsis PI* was overexpressed in wild-type rice. These findings suggest that increased ubiquitous *PI* activity is detrimental to anther development. To uncover genes whose (in)direct regulation may contribute to these phenotypes, we combined the

genome-wide identification of OsMADS2 binding regions (ChIP-Seq) with transcriptome profiling (RNA-Seq). These analysis uncovered several OsMADS2 target genes that are implicated in lodicule and stamen development and in controlling floral organ number, *e.g.*, *PECTIN METHYLESTERASE 24* (*PME24*), *GLYCOSIDE HYDROLASE 9B16* (*GH9B16*), *TAPETUM DEGENERATION RETARDATION* (*TDR*), *SPOROCYTELESS* (*SPL*), *FLORAL ORGAN NUMBER 1* (*FON1*), *YUCCA*3 and *YUCCA7*. Altogether, our results provide insights on the underlying molecular mechanisms of rice *PI* paralogs in floral organ specification, thereby expanding our understanding of their function as well as their conservation and diversification.

Keywords: *OsMADS2*, *OsMADS4*, *PISTILLATA*, lodicule, petal, stamen, floral organ number

Introduction

In flowering plants (angiosperms), floral organs are arranged in four concentric whorls. The identity of floral organs that develop in these whorls is controlled by the combinatorial action of homeotic transcription factors belonging, with few exceptions, to the MIKC-type MADS-domain family (Lohmann and Weigel, 2002; Krizek and Fletcher, 2005). Thirty years ago, the ABC model of floral organ patterning was proposed and later expanded to become the ABCDE model, comprising five homeotic classes of transcription factors: A, B, C, D and E (Coen and Meyerowitz, 1991; Favaro et al., 2003; Pinyopich et al., 2003; Krizek and Fletcher, 2005). Although not strictly conserved across all angiosperms, this model provides a baseline for understanding floral development and for gauging functional divergence. According to the ABCDE model, specification of the second and third whorl organs (petals and stamens), in eudicots, requires a pair of related B-class homeotic genes. These are *APETALA3* (*AP3*) and *PISTILLATA* (*PI*) in the model plant *Arabidopsis thaliana*, and *DEFICIENS* (*DEF*) and *GLOBOSA* (*GLO*) in *Antirrhinum majus.* Not surprisingly, studies in maize and rice demonstrated that B-class genes are similarly required for specifying the identity of second and thirs whorl organs, lodicules and stamens (Ambrose et al., 2000; Nagasawa et al., 2003; Prasad and Vijayraghavan, 2003; Yadav et al., 2007). These results support the interpretation that lodicules are analogues of eudicot petals and indicate some shared genetic control of lodicule and petal development. However, the remarkable morphological and functional differences of these organs plausibly indicate that their developmental differentiation pathways are very different. Understanding the mechanisms underlying floral organ diversification has long been a challenge (Schwarz-Sommer et al., 1990; Irish, 2010). With respect to lodicule and stamen

development, the rice genome has two *PI* paralogs, named *OsMADS2* and *OsMADS4* (Chung et al., 1995). The phenotypes of lodicules and stamens of single and double knockdown plants, *i.e.*, *osmads2dsRNAi*, *osmads4dsRNAi*, and *osmads2;osmads4dsRNAi* suggested unequal redundancy for lodicule but complete redundancy for stamen development, respectively (Prasad and Vijayraghavan, 2003; Yao et al., 2008). Yet, the underlying cause of functional divergence in lodicule development is unknown. Furthermore, while the maize *PI* paralog *Zmm16* was shown to partially rescue the *Arabidopsis pi-1* mutant phenotype (Whipple et al., 2004), the extent of conservation between the rice *PI* paralogs and *AtPI* is not known.

Insights into the molecular function of transcription factors come from the identification of their target genes and the genome-wide determination of their binding regions. In the monocot models maize and rice, reports on such studies are increasing. Although a previous study on downstream targets of OsMADS2 suggested a diversification compared to AtPI, the study employed RNA interference-mediated gene silencing (RNAi) to downregulate *OsMADS2* and examined transcriptomic changes in a pool of floral tissues encompassing a broad range of developmental stages (inflorescences of 0.5-4 cm length) using the then available 22,000 probe-based microarray (Yadav et al., 2007). The transcriptome data from this study demonstrated that a sizable fraction (9%) of OsMADS2 targets function in diverse aspects of cell division control. Here, we first generated null alleles of *OsMADS2* by genome editing, carried out a detailed phenotypic analysis, and performed developmentally staged transcriptome profiling. To unravel the gene regulatory network underlying the sub-functionalized B-function of OsMADS2, this transcriptome analysis was coupled with a determination of the genome-wide DNA occupancy of the OsMADS2 protein in panicles containing developing florets. Furthermore, we employed genetic complementation assays and examined the consequences of ubiquitous overexpression of *AtPI* in wild-type rice plants to better understand the extent and cause of divergence between different *PI* orthologs/paralogs. Our data emphasize the importance of investigating homeotic genes outside the core eudicot models to gain novel insights into their evolutionary conservation and diversification. This study reports novel process that are regulated by OsMADS2, such as flowering time, floral organ number, and cell wall organization and elucidates mechanisms by which rice *PI* paralogs control floral organ number, floral organ identity, and tissue differentiation.

Results

Mutations in *OsMADS2* alter lodicule identity without affecting the stamens

OsMADS2 was first demonstrated to regulate rice lodicule identity by Prasad and Vijayraghavan (2003) using RNAi. Despite drastic downregulation, RNAi may only phenocopy a partial loss-of-function mutant and, as known from other studies employing RNAi, could trigger the unintended silencing of homologous genes (Jackson et al., 2003; Kouzai et al., 2014). Therefore, not unexpectedly, varying roles in stamen development have been reported for *OsMADS2*. While the *OsMADS2 dsRN*Ai lines generated by Prasad and Vijayraghavan (2003) had a normal stamen morphology and near normal fertility with some manual assistance, Yao et al. (2008) described low fertility attributed to poor anther dehiscence. Thus, the extent of functional redundancy between the *PI* paralogs *OsMADS2* and *OsMADS4* with respect to stamen development is not clear and these reports highlight the necessity of studying developmental phenotypes in null mutants. To resolve the role of *OsMADS2* in lodicule and stamen development, we generated multiple loss-of-function alleles using CRISPR/Cas9-based genome editing. The *osmads2*$^{i1/i1}$*-dbd* allele with a single base pair (bp) insertion caused a frameshift within the MADS DNA binding domain (DBD), leading to a premature stop codon. The *osmads*$^{i1/i1}$, *osmads2*$^{d2/d2}$, and *osmads2*$^{d8/d8}$ alleles contained a 1 bp insertion, a 2 bp deletion, and an 8 bp deletion, respectively and created early stop codons within the coiled-coil keratin-like domain (K domain) that is involved in oligomerization (Supplemental Figure 1, A-C). Segregation analyses of different *osmads2* mutant alleles in heterozygous and biallelic combinations showed no evidence of allelic drive as they segregated to expected Mendelian ratios in the T4 progeny (Supplemental Data Table 1).

To assess the role of *OsMADS2* in floret development, a morphological characterization of pre-anthesis, mature spikelets (Itoh et al., 2005) was performed on homozygotes for all these alleles and on heterozygous *osmads*$^{+/d8}$ plants. For detailed investigations, we focused on *osmads*$^{d8/d8}$ homozygous plants using Scanning Electron Microscopy (SEM) and histological sectioning. Florets of the different homozygous mutants exhibited abnormally long lodicules. Some common phenotypes were overgrowth of the lodicule distal ends (Figure 1, A *vs.* B; Supplemental Figure 2, G *vs.* H-K), abnormally elongated epidermal layer cells that are characteristic of marginal tissue of the palea (MTP) or of the sterile lemma (SL; Figure 2, G-J), and reduced thickness of the lodicule attributed to a decreased number of parenchyma cell layers (Figure 3, E *vs.* F). In wild-type lodicules, the vascular bundles are arranged in two rows

along the transverse axis. Strikingly, mutant lodicules exhibited a reduced number of vascular bundles and disruption of their distinct arrangement (Fig. 3, E *vs.* F; Supplemental Figure 3, A *vs.* B). These abnormal phenotypes indicate a partial homeotic transformation of the lodicule to MTP or SL, which is, to a large extent, similar to the phenotype observed in *OsMADS2* RNAi transgenic florets (Prasad and Vijayraghavan, 2003; Yadav et al., 2007). However, compared to *OsMADS2* RNAi lines, *osmads*$^{d8/d8}$ mutants exhibited stronger lodicule abnormalities. In this regard, in one instance (N=1/6), by SEM we found trichomes on the adaxial epidermal cells of the lodicule (Figure 2M). In transverse histological sections, we observed occasional lignifications of the lodicule cell walls as indicated by blue-greenish coloration upon tolidine blue staining. In addition, in these sections we saw a change of the bricklike shape of parenchyma cells into a polygonal shape (Figure 3, E *vs.* F and I *vs.* J). A consequences of these lodicule differentiation defects is that some *osmads2* florets remain partially open after anthesis (11/68 in *osmads2* compared to 13/117 in the wild type [WT]). Unlike lodicules, gross stamen morphology and pollen viability in *osmads2* mutants were apparently normal and mutant plants had a normal fertility as compared to WT (Figure 1, A-D and I; Figure 3, K *vs.* L; Supplemental Figure 4, B and H). Infrequently (<1%), one of the six stamens in a floret had a short filament and white, empty anthers (Supplemental Figure 2B). Rarely, we also observed lodicule-stamen or stamen-carpel chimeric organs and a partial 'superwoman' phenotype, in which the stamen number is reduced concomitant with an increase in carpel number (Figure 1C; Supplemental Figure 2D). Strikingly, *osmads2*$^{+/d8}$ heterozygous florets infrequently also showed lodicule elongation and an increased number of floral organs (Supplemental Figure 2, E and F). We hypothesize that these infrequent phenotypic variations in heterozygous plants arise from stochastic fluctuations in gene expression (Elowitz et al., 2002; Balázsi et al., 2011), the amplitude of which is magnified upon loss of gene duplication.

Floral phenotypes of the *osmads2*$^{d8/d8}$ null mutant

Although all homozygous *osmads2* mutants showed similar lodicule phenotypes, we decided to focus on *osmads2*$^{d8/d8}$ for detailed phenotypic and molecular studies. During inflorescence development, the *OsMADS2* transcript level in the *osmads2*$^{d8/d8}$ mutant was reduced ~ 4-fold as compared to WT (Supplemental Figure 1D). Either the mutant transcript with a premature stop codon undergoes nonsense-mediated mRNA decay or the expression levels of *OsMADS2* are maintained in a positive transcriptional self-activation loop. Importantly, OsMADS2 is not detected in panicle nuclear protein lysates on a Western blot using an affinity-purified anti-OsMADS2 antibody (Supplemental Figure 1E). Altogether, these data suggests that

osmads2$^{d8/d8}$ is a null mutant. To characterize vegetative and floral phenotypes of *osmads2*$^{d8/d8}$, mutants were grown alongside WT plants in a greenhouse. During vegetative growth, we did not observe any discernable abnormality in *osmads2*$^{d8/d8}$ mutants. Surpisingly, however, *osmads2*$^{d8/d8}$ plants commenced the floral transition nearly 15 days earlier than the WT (Supplemental Figure 5A). Upon flowering, we analysed spikelet phenotypes and found that *osmads2*$^{d8/d8}$ florets displayed, at low penetrance (5.8%), an increase in the number of inner floral organs. In this respect, 1.8% of the florets had 3 lodicules (Figure 1D), 5.4% showed 7 stamens (Figure 1D), and 1.8% had 2 carpels. As of a result, the average number of floral organs internal to lemma and palea increased from 9 in WT (n= 138) to 9.08 in *osmads2*$^{d8/d8}$ (n = 222, P value = 0.0198, *t*-test), suggesting an enlarged floral meristem size in the mutant. Like *osmads2*, mutants disrupting the maize *PI* ortholog, *sterile tassel silky ear1* (*sts1*), exhibited a varying number of ectopic organs in the third whorl (Bartlett et al., 2015), suggesting a conserved function of grass *PI* orthologs in controlling floral organ number. Interestingly, the ectopic lodicule in the *osmads2* $^{d8/d8}$ mutant was positioned in the other half of the second whorl, opposite to the normal lodicules (Figure 1D; Supplemental Figure 3C). This indicates a previously unknown role of *OsMADS2* in mediating the asymmetric phyllotaxy of organs in the second whorl. Occasionally, we observed spikelets where the inner SL became green and enlarged suggesting transformation into palea- or lemma-like organ (Supplemental Figure 2C). Taken together, these results indicate the CRISPR/Cas9 generated *osmads2* mutants not only display stronger lodicule identity phenotypes when compared to *OsMADS2* dsRNAi lines, but the null alleles also revealed previously unreported phenotypes, pointing to additional processes that are regulated by *OsMADS2*. Importantly, the earlier flowering time and the increased number of floral organs imply a functional divergence of *OsMADS2* from its distant ortholog *AtPI*.

Ubiquitous overexpression of the paralog *OsMADS4* complements *osmads2* phenotypes

OsMADS2 and *OsMADS4* are *PI* clade MADS-box gene paralogs on rice chromosomes 1 and 4, respectively. They encode proteins that are 83.7% identical and 92.3% similar. Studies on *OsMADS4* reported some variations with respect to its role in the regulation of lodicule and stamen development. Upon knockdown of *OsMADS4*, Kang et al. (1998) observed homeotic transformations of lodicules to palea/lemma-like structures and of stamens to carpel-like structures. We have re-examined *OsMADS4* function in an independent study employing a dsRNAi cassette specific to the *OsMADS4* locus. In dsRNAi *OsMADS4* transgenic line #1 (termed *osmads4kd* hereafter), we found *OsMADS4* and *OsMADS2* transcripts levels in 2 cm

panicles to be ~ 8-fold and ~ 2-fold downregulated, respectively (Supplemental Figure 6). Since the dsRNAi cassette is *OsMADS4*-specific, we conclude that OsMADS4 positively regulates the expression of *OsMADS2*, similar to what is known with respect to feedback regulation between the *Arabidopsis* B-class genes *PI* and *AP3* (Zik and Irish, 2003). Despite a robust downregulation of *OsMADS4* in the *osmads4kd* line#1, the florets were normal and plants were fertile (Figure 1E and I). This finding supports the hypothesis of Yao et al. (2008) that the superwoman phenotype of *OsMADS4* antisense lines described by Kang et al. (1998) is likely caused by the unintended knockdown of the *OsMADS2* paralog, since they used a full length antisense *OsMADS4* cDNA. Collectively, the phenotypic characterization of *osmads2* and *osmads4kd* indicate that the rice *PI* paralogs are fully redundant with respect to stamen specification but have divergent roles for lodicule development.

To better understand the extent of the functional divergence of the rice *PI* paralogs, we ubiquitously overexpressed *OsMADS4* in the *osmads2* mutant background. The *osmads2 OsMADS4-OX* transgenic plants (termed *osm2 OsM4-OX* hereafter) had normal first and fourth whorl organs (Figure 1F). Furthermore, *OsMADS4* overexpression complemented the different floral phenotypes of *osmads2* mutants, such as abnormal lodicules and an aberrant floral organ number, but the *osm2 OsM4-OX* plants exhibited abnormal, crescent-shaped anthers (Figure 1F). Transverse histological sections of lodicules showed a normal arrangement of the vascular bundles (Supplemental Figure 3, A *vs.* B and D). However, sections through the anthers revealed their underdevelopment in *osm2 OsM4-OX* plants. Unlike in WT, where the anthers are organized into four synchronized locules, the anthers of *osmad2 OsMADS4-OX* plants frequently exhibited defects in one or two locules (Figure 3, K and L *vs.* M). Consistent with the defects of the anthers, pollen viability and seed set was significantly reduced in comparison to WT (Figure 1I; Supplemental Figure 4, C and F). We conclude that a precisely fine-tuned expression of *OsMADS2* and *OsMADS4* is required for normal anther development.

In the T1 generation of *osm2 OsM4-OX* lines, we identified azygous segregants without the *OsMADS4-OX* transgene, which we refer to as *osmads2 OsMADS4 azygous.* As expected, these plants exhibited lodicule abnormalities typical of *osmads2* mutants. We recorded the flowering time of *osmads2 OsMADS4-OX* and *osmads2 OsMADS4 azygous* plants, with the latter flowering approximately two weeks earlier (Supplemental Figure 5B). This finding indicates that the ubiquitous overexpression of *OsMADS4* complemented the *osmads2* early flowering phenotype, revealing a unique function of the rice *PI* paralogs in regulating the floral transition.

To better understand the underlying basis of early flowering in *osmads2* mutants, we inspected the expression of B-class MADS-domain transcription factors in the vegetative shoot apical meristem (SAM). RT-qPCR results showed that *OsMADS2* expression is ~ 3-fold downregulated in SAMs of seedlings 7 days post-germination (Supplemental Figure 5C). An analysis of publicly available RNA-Seq data from 6-week-old SAMs of rice (Gómez-Ariza et al., 2019) and 9-day-old SAMs of *Arabidopsis* (Klepikova et al., 2015) showed that *OsMADS2* and *OsMADS16* were expressed in the SAM, while *OsMADS4*, *Arabidopsis PI* and *AP3* were not (Supplemental Figure 5E). Furthermore, the spatio-temporal expression of *OsMADS2*, as reported in the riceXPro database (Sato et al., 2013), showed a relatively high transcript level in the reproductive stem (Supplemental Figure 5E). Additionally, the presence of the OsMADS2 protein in leaves can be inferred from Uji et al. (2019), who identified it as an interacting protein of OsVQ13. Taken together, these results suggest that *OsMADS2* expression in the SAM prevents a precocious floral transition and identify a diverging, novel function of *OsMADS2* that differentiates it from *OsMADS4* and *Arabidopsis PI*. Our data on the complementation of different *osmads2* mutant phenotypes suggest that the functional divergence among rice *PI* paralogs can likely be attributed to changes in *cis*-regulatory elements that alter their domain and level of expression, rather than changes in the nature of their biochemical function as B-class transcription factors.

OsMADS4 **supports lodicule function and identity**

Considering the functional redundancy among the rice *PI* paralogs and to better understand their functions in spikelet development, we generated a double mutant by crossing *osmads4kd* and *osmads2*$^{d8/d8}$ plants. To facilitate crossing, the parents were grown side-by-side in the same pots. Mutant *osmads2*$^{d8/d8}$ plants flowered approximately 2 weeks earlier as compared to *osmads4kd* line (Supplemental Figure 5F). This reiterates the precocious flowering of *osmads2*$^{d8/d8}$ and indicates divergence of *OsMADS2* from *OsMADS4* in regards to this trait. With parents *osmads2*$^{d8/d8}$ and *osmads4kd* grown such that they were synchronized for anthesis, we successfully bred the desired cross. The F1 plants, designated as *osmads2*$^{+/d8}$ *osmads4kd*, set seed upon self-fertilization. Among their F2 progeny, we identified *osmads2*$^{d8/d8}$ *osmads4kd* plants that had no discernible vegetative abnormalities, but floral development was dramatically altered. The lodicules were elongated and severely flattened throughout their proximal-distal axis (Figure 1G and H). As a consequence of this severe lodicule misspecification as a glume- or leaf-like organ, all florets remained unopened. Based on severity of the phenotype in third whorl organs, the *osmads2*$^{d8/d8}$ *osmads4kd* plants were

classified into two groups: Florets of group I plants displayed strong superwoman phenotype, with all or the majority of stamens being replaced by ectopic carpels (Figure 1G; Figure 3C). Florets from group II displayed a milder superwoman phenotype, with most of the stamens present but sterile (Figure 1H; Figure 3D; Supplemental Figure 4, E-G). We hypothesize that variation in the superwoman phenotype may arise from differences in the degree of *OsMADS4* downregulation. Segregation analysis of the *OsMADS4 dsRNAi* transgene across generations indicates that the T-DNA integrated at a single genomic locus as it segregated in ~ 3:4 ratio (65/89 plants carried the *OsMADS4 dsRNAi* transgene). Amplifification and sequencing of the genomic region flanking this T-DNA showed that it integrated in an intergenic region on chromosome 8 (Supplemental Figure 7A). Using insertion site-specific PCR, we showed that group I (average stamen number 2.4) and group II (average stamen number 5.3) phenotypes are associated with the *OsMADS4* dsRNAi transgene being homozygous and hemizygous, respectively (Supplemental Figure 7, A and B; Supplemental Table 2). Interestingly, in the unopened *osmads2 osmads4kd* florets, the stamen filaments did not elongate. Moreover, the emergence of all *osmads2 osmads4kd* inflorescences from the flag leaf sheath (panicle enclosure) was compromised, suggesting poor rachis elongation (Figure 1J). Together, the panicle enclosure phenotype and the failure of stamen filament extension suggest compromised hormone signaling regulating cell elongation in *osmads2 osmads4kd* inflorescences.

We also observed that the inner SL in many *osmads2 osmads4kd* spikelets were overgrown and greenish (44/765 as compared to 1/508 in WT, P value < 0.0001, Fisher's exact test). Such a phenotype, had also been noted at very low penetrance in *osmads2*$^{d8/d8}$ single mutants (Supplemental Figure 2C). To investigate the identity of the abnormal organs, spikelets from *osmads2 osmads4kd* panicles were examined by SEM and histological sectioning. Compared to the *osmads2*$^{d8/d8}$ single mutant, *osmads2 osmads4kd* lodicules exhibited more severe abnormalities: The epidermal cells of the proximal and distal parts of the malformed lodicules were elongated and midveins were observed along the proximal-distal axis (Figure 2K and Figure 3, C and H). Furthermore, the number of vascular bundles and the thickness of the lodicules were drastically reduced, and the adaxial side was lined with bubble-shaped cells resembling those on the adaxial surface of the lemma/palea (Figure 3, C, D, G and H). Importantly, cells of *osmads2 osmads4kd* lodicules exhibited increased cell wall lignification as indicated by a greenish-blue coloration upon toluidine blue staining (Figure 3, D and G). Transverse section of anthers from group II florets showed a prolonged presence of the tapetum layer, which undergoes cell death in the WT (Supplemental Figure 3G). This retardation of

tapetum decay likely contributes to pollen unviability and male sterility in these plants. Moreover, sections of the abnormally enlarged SL revealed three vascular bundles, suggesting that they acquired a palea-like identity (Figure 3, N *vs.* O). Compared to the *osmads2* single mutant, in which only 5.8% of the florets had an increased number of floral organs, ~ 44% of *osmads2*$^{d8/d8}$ *osmads4kd* florets (58/130) had an increased number of inner organs (Figure 1H; Figure 3, C and D). We interrogated the size of the floret meristem (FM) in developing spikelets from WT, *osmads2*, and *osmads2*$^{d8/d8}$ *osmads4kd* panicles. Interestingly, SEM analyses showed that *osmads2* florets have a slight increase in FM size as compared to the WT. Notably, the FM size in the *osmads2*$^{d8/d8}$ *osmads4kd* florets at spikelet stage Sp6 was clearly larger than that in either WT or *osmads2* single mutant florets (Supplemental Figure 8). The enlarged FM size in *osmads2*$^{d8/d8}$ *osmads4kd* spiklets is reminiscent of the FM enlargment in the *osmads16/spw1* mutant as evident from SEM micrographs in Yun et al. (2013). Altogether, we conclude that OsMADS4 regulates the identity and differentiation of lodicules and stamens likely by contributing to a functional B-class complex in the absence of OsMADS2, which is in general agreement with the hypothesis proposed by Yoshida et al. (2007). Importantly, the downregulation of *OsMADS4* in the *osmads2* null mutant background uncovered previously unreported roles for the rice *PI* paralogs in rachis elongation, cell wall metabolism, FM size, floral organ number, and SL development.

Rice *PI* paralogs are required for embryo sac development and suppress parthenocarpy

Florets of *osmads2 osmads4kd* lines were male sterile due to either the absence of male organs in group I or the lack of viable pollen in group II (Figure 1G and Supplemental Figure 4, E-G). To test female fertility of *osmads2 osmads4kd* plants, carpels from both phenotypic groups were dusted with WT pollen. Surprisingly, there was a complete failure of seed set in these crosses (Figure 4A), despite the presence of ovule-like structures within the central fourth whorl carpel and some of the ectopic carpels in *osmads2*$^{d8/d8}$ *osmads4kd* florets (Figure 3, C and D). These data suggest that the sterility of *osmads2 osmads4kd* florets is not merely due to defective male organs. A closer inspection of *osmads2*$^{d8/d8}$ *osmads4kd* ovaries revealed that some of the ovule-like structures bear undifferentiated nucellar tissue lacking differentiated embryo sacs (Supplemental Figure 9, compare A-C *vs.* H-J and D-G *vs* K-O). Other observed ovule abnormalities, that also underlie female sterility, include embryo sac degeneration, embryo sacs without an egg apparatus, embryo sacs without female germ unit, embryo sacs without antipodal cells, embryo sacs without polar nuclei, and embryo sacs that lack antipodal cells and have misplaced polar nuclei (Figure 4, compare B *vs.* D-K). Interestingly, a few

ovules (3/10) of *osmads2*$^{d8/d8}$ *osmads4kd* florets from group II have apparently normal embryo sacs (Figure 4C), suggesting they may possess a low female fertility or that their infertility is due to defects during fertilization or seed/fruit development. These results are consistent with the rice *spw1-1* mutant being female sterile, contrasting with the *Arabidopsis ap3* or *pi* mutants, which are female fertile (Krizek and Meyerowitz, 1996; Nagasawa et al., 2003). Surprisingly, the sterile *osmads2 osmads4kd* florets of both groups displayed ovary expansion; a response that is normally triggered by fertilization (Figure 5, A-C). Eventually, these expanded ovaries shrunk and aborted (Figure 5D). Closer inspection showed that they lacked endosperms and embryos (Figure 5, E and F *vs* G; H *vs* I and J), suggesting that the fruit development initated without formation of the products of double fertilization, a phenomenon referred to as parthenocarpy. Altogether, these results point to previously unreported roles of the rice *PI* paralogs in embryo sac and seed/fruit development.

Ubiquitous overexpression of *Arabidopsis PI* in rice is insufficient to trigger homeotic transformation of floral organs

Arabidopsis PISTILLATA (*AtPI*) and rice *OsMADS2* share 50% and 80 % amino acid identity and similarity, respectively. We ubiquitously overexpressed *AtPI* cDNA (Supplemental Figure 10A) in WT rice to examine the extent of conservation of B-class floral development functions. Transgenic lines designated as *AtPI-OX* had a low frequency (n = 3/83) of one to three extra stamens (Supplemental Figure 2L). As seen for *osmads2 OsMADS4-OX* lines, plants ubiquitously expressing *AtPI* (Supplemental Figure 10B) had apparently normal first and fourth whorl organs. Yeast two-hybrid (Y2H) assays and RNAi analysis (Yao et al., 2008; Kong et al., 2019) showed that OsMADS16, the rice AP3 ortholog, interacts with either of the rice PI orthologs OsMADS2 or OsMADS4 to form the functional B-class complexes. *OsMADS16* transcripts are not detected in first or fourth whorls organ primordia or developing organs (Nagasawa et al., 2003). Our experiments with ubiquitous expression of either *AtPI* or *OsMADS4* in rice transgenics were, predictably, insufficient to trigger rice floret homeotic organ transformations in whorls one or four, most likely due to the absence of a functional B-class heteromeric complexes (AtPI/OsMADS4-OsMADS16). Like seen in florets of *osmads2 OsMADS4-OX* plants, underdeveloped anthers, reduced pollen viability and seed setting were also observed in *AtPI-OX* rice transgenics (Figure 1I; Supplemental Figure 3E; 4H). Despite the reduced pollen viability, closer inspection of post-anthesis *PI-OX* florets revealed ovary expansion in majority of the florets. Unlike WT florets, many of these expanded ovaries, containing transparent liquid and of comparable size to mature seeds, failed to develop starchy

endosperm and ultimately aborted (Supplemental Figure 2M). In flowering plant, ovary expansion can be triggered by either fertilization or by phytohormone-mediated parthenocarpy. Further, a similar phenotype of rice *PI-OX* ovaries was seen in *osgcs1* mutant where pollen tube content release inside the ovule triggered ovary enlargement and sucrose unloading without fertilization (Honma et al., 2020). This phenomenon is termed pollen tube-dependent ovule enlargement morphology (POEM). To understand the underlying cause of *PI-OX* ovary phenotype, we tested consequences of emasculation on ovary development. The emasculated *AtPI-OX* florets failed to develop seeds and did not show ovary expansion indicating that the ovary phenotypes seen in *AtPI-OX* is pollination dependent and not attributed to phytohormone-mediated parthenocarpy. We further examined expanded ovaries and found that they lack embryo and endosperm suggesting that they were not fertilized (Supplemental Figure 10C). Further, we analyzed this transparent liquid in the ovules by liquid chromatography-mass spectrometry (LC-MS) and found that it majorly constitutes sucrose (Supplemental Figure 10D). Together, these results suggest that ubiquitous *AtPI* overexpression in WT rice triggers POEM, likely due to male or female gamete defects.

Mapping OsMADS2 genome-wide occupancy in developing florets

To understand the role of OsMADS2 as a regulator of rice floral organ development, we mapped its genome-wide binding sites in panicle tissues with florets in a wide range of developmental stages by Chromatin ImmunoPrecipitation followed by deep sequencing (ChIP-Seq). For this experiment, inflorescences between 0.3-2cm were used with anti-OsMADS2 antibodies, the retrieved immuno-precipitated DNA sequenced, and the raw data processed as described in materials and methods. After alignment of the sequences, peaks of DNA occupancy were called by comparing enrichment of aligned reads from the IP over that in mock pull down (IgG). Peaks called from two independent replicates (24169 and 10603 respectively) were mapped with respect to gene transcription start site (-3000 to +3000 from the TSS). We observed high enrichment of binding sites in close proximity of the TSS (Figure 6A), as reported for other transcription factors, including *Arabidopsis* PI and AP3 (Kaufmann et al., 2009; Winter et al, 2011; Wuest et al., 2012). We identified 1536 confident peaks overlap in the two biological replicates that show ≥ 2-fold enrichment at FDR ≤ 0.05 when compared to the mock chromatin pull down. These confident peaks were assigned to 2589 genes and are located in their vicinity up to 4000 bp from either start (TSS) or end of the gene (end of the last exon) (Supplementary Dataset 1). To identify sequence motifs likely bound by OsMADS2,

MEME-ChIP from MEME suite (Machanick and Bailey, 2011) was performed on DNA set from those 1536 confident peaks and the significantly enriched motifs (E value <= 0.05) were retrieved. These motifs included CGG-repeats (5'GCGGCGGCGGCGRC3'), T-Track (TTTTYTTTTTTTTYT), G-repeats (5'GSAGVAGVAGSWGGV3') and CArG-like (5'TATACAAAGTTTGYA3') *cis* elements (Figure 6B and Supplemental Figure 13A). Enrichment of these motifs at these OsMADS2 target loci was further investigated by scanning 400 bp segments up to 3000 bp upstream or downstream of the peak midpoint. Our analyses indicated enrichment of these motifs in 400 bp peak region of target loci compared to the flanking sequences (Figure 6B). Surprisingly, no canonical CArG box (5'CC(AT)6GG3') motifs were retrieved from MEME analyses. Further our analyses showed that canonical CArG motifs are not also enriched in 400 bp peak regions as compared to the flanking sequences (400 bp windows up to 3000 bp from the peak region, Supplemental Figure 13B). In *Arabidopsis*, the genome binding sites for PI/AP3 (Wuest et al., 2012) are enriched for G-boxes (5′-CACGTG-3′) and GA repeats (5′-GAGAGAGH-3′). Our analyses showed that these motifs are highly enriched in peak regions compared to their flanking sequences (Figure 6B). Although MADS domain proteins are known to bind CArG box sequences, they have been shown to bind non-CArG box sequences *in vitro* (Hill et al., 1998). Together, while our analyses do not exclude OsMADS2 binding to canonical CArG elements, it rather suggests preferential association to chromatin that are enriched with other motifs including GCC-Repeat and CArG-like sequences. To validate the ChIP-Seq results, we tested a number of loci associated with the confident peaks from the genome-wide analyses by ChIP-qPCR on two independent chromatin preparations. These loci were chosen based on their annotations with functions relevant to *osmads2* null mutant phenotypes. In this respect, using inflorescence tissues of 0.5-1 cm, we validated OsMADS2 binding to *GLYCOSIDE HYDROLASE 9B16* (*GH9B16*), *HEAT STRESS TRANSCRIPTION FACTOR C1b* (*HSFC1B*), *PROLIFERATING CELL FACTOR 2* (*PCF2*), *CYCLIN-P4-1-LIKE* (Os07g0231500), *ETHYLENE RESPONSE FACTOR 61* (*ERF61*) and *PROTEIN TRANSPORTER 2* (*PTR2*, Figure 7). In 1-2 cm inflorescence, we validated OsMADS2 binding to *EGL1* (Supplemental Figure 14). Both *PCF2* and *CYCLIN-P4-1-LIKE* functions in cell division are related to the abnormalities in floral meristem size, organ number and lodicule shape which are seen in *osmads2* mutant. *EGL1* and *GH9B16* encode endo-(1,3;1,4)-β-glucanases and are proposed to aid the partial hydrolysis of cell wall to permit turgor driven cell expansion (Cosgrove et al., 1999; Akiyama et al., 2009; Xie et al., 2013). Hence, they represent important OsMADS2 target genes that facilitate normal lodicule development and physiology. On the other hand, genes such as *PTR2* can explain the roles

played by OsMADS2 in contributing to vascular patterning (Li et al., 2015). *HSFC1B*, on the other hand, as a target gene of OsMADS2 (Figure 7; Figure 8, B-D), may improve thermotolerance under high temperature to ensure normal gametophyte development. Further, based on its role in osmotic regulation (Schmidt et al., 2012), it may aid lodicule dilation and shrinking, during and after anthesis; a physiological process derailed in *osmads2*$^{-/-}$ *osmads4kd* double mutant florets. Together, these results shed insight on the molecular roles of OsMADS2 in rice floral development by uncovering OsMADS2-bound loci that, among many functions, can control cell wall organization, vascular development, osmotic regulation and cell proliferation.

Global transcriptome profiling of *osmads2*$^{d8/d8}$ mutant in developing inflorescence

The role of OsMADS2 as a transcription factor in directing downstream gene expression for specific developmental outcomes was studied by examining its global effects on transcriptome of developing panicles with florets. We compared the transcriptomes of *osmads2*$^{d8/d8}$ and WT panicles by RNA sequencing (RNA-seq; Figure 8; Supplementary Dataset 2) in tissues combined to form three developmental pools. The three pools of tissues comprised immature inflorescences: 0.2-0.5 cm (termed early here on), 0.5-1 cm (termed middle here on) and 1-2 cm (termed late here on). The early pool would contain florets at stages of floral meristem specification and floral organ primordia initiation and patterning. The middle pool mostly constitutes florets with differentiating organs and the late pool constitutes florets undergoing organ growth and early gametogenesis. For each developmental pool, RNA-Seq was done for two biological replicates from *osmads2*$^{d8/d8}$ and three biological replicates of WT. The differentially expressed genes (DEGs) were derived by comparing *osmads2*$^{d8/d8}$ *vs.* WT transcriptome datasets applying a fold-change ≥ 2 and FDR ≤ 0.05. Compared to WT, 376 genes, 2215 genes and 169 genes were significantly deregulated in mutant tissues in early, middle and late stages, respectively (Supplementary Dataset 2). The higher number of DEGs in tissues binned as “middle stage” is consistent with higher expression level of *OsMADS2* itself in the tissues of this stage (Supplemental Figure, 11A) and imply important roles of OsMADS2 during floral organs differentiation. Among DEGs, 314 genes, 1888 genes and 139 genes were downregulated in *osmads2*$^{d8/d8}$ tissues at early, middle and late developmental stages, respectively. The increased number of downregulated genes in mutant tissues indicates that OsMADS2 acts majorly as an activator for transcription of its downstream genes. DEGs that are common to different developmental pools were identified by overlapping the three datasets. Expectedly, the common genes between any two datasets were mostly consistent with

few dynamic exceptions being upregulated in one stage and down regulated in the other (Supplemental Figure 11, B and C). Interestingly, *OsMADS2* was downregulated in all the stages. Inspection of Integrated Genome Viewer (IGV) alignment for *OsMADS2* locus revealed that both wild type and mutant are having comparable level of mapped intronic reads from pre-mRNA (Supplemental Figure 11D). Since changes in reads mapped to introns mirror transcriptional changes (Gaidatzis et al., 2015), this result suggests that reduction in *osmads2*$^{d8/d8}$ mRNA is likely attributed to post-transcriptional event such as Nonsense Mediated Decay (NMD) rather than loss of transcriptional auto-activation by feedback loop. Interestingly, in all RNA-seq libraries of WT, *OsMADS2* expression levels were higher than *OsMADS4* (Supplemental Figure 11E), suggesting significant divergence in the *cis* DNA elements that drive the expression of these paralogous genes. To uncover different molecular functions, biological processes and cellular components controlled by OsMADS2, gene ontology (GO) enrichment analysis (Figure 8A; Supplementary Dataset 3) was conducted on DEG datasets that were first sub grouped as activated (by OsMADS2 in WT) or repressed (by OsMADS2 in WT). These analyses revealed enrichment for “DNA binding” and “transcription factor activity” in the activated/positively regulated gene subsets (lower transcript levels in the *osmads2*$^{d8/d8}$ mutant) in tissues at the early and middle stages. The enrichment of “transcription factor activity” in the activated (positively regulated by OsMADS2) gene subsets, is consistent with OsMADS2 acting, largely, as a transcription activator of downstream genes. Interestingly, the enrichment analysis uncovered several GO terms that relate to the role of OsMADS2 in lodicule and stamen development. In this respect, the OsMADS2 activated gene subset in the late floret development stage was enriched for “anther development”, while the repressed gene subset (higher transcript levels in *osmads2*$^{d8/d8}$ mutant) in the middle stage was enriched for “carpel formation”. This likely explain how this rice PI clade B-class gene promote stamen development and suppress carpel formation in WT rice florets. With respect to lodicule development and function, cell wall plasticity and water transport are both required for the rapid swelling and shrinking that is timed during and after anthesis. Osmotic homeostasis also aids this process. Interestingly, in OsMADS2 repressed DEG gene subsets we note enrichment for “plant type cell wall” during late stage of development and “lignan biosynthesis” processes during middle stages of development. Notable in the activated gene subset is the enrichment for genes with functions related to “response to water deprivation” during middle stages of development. Phytohormones control both cell proliferation and organ differentiation. Remarkably, “auxin biosynthetic process” was enriched in the repressed DEG gene subset of early-stage florets (Figure 8A; Supplementary Dataset 3). Therefore, it is plausible that the

increased expression of *OsYUCCA3* and *OsYUCCA7* in *osmads2* florets in this stage could be promoting floral whorls over-proliferation and consequent effect of increase in floral organ number. We scrutinized the DEGs that are annotated with predicted functions, and in few instances identified genes that were functionally characterized. Taken into account the redundant functions of *OsMADS2* with *OsMADS4*, we present here two more functionaly relevant genes despite their statistically lower threshold value (≥ 1.8-fold change regulation at q value ≤ 0.05). The precocious flowering in *osmads2*$^{d8/d8}$ null mutant, may be linked to lowered abundance of *CONSTANS-like 15* (*OsCOL15*), *OsGIGANTEA* (*OsGI*), *OsMADS55* (logFC = -0.986, FDR = 0.03) and *RICE CENTRORADIALIS 2* (*RCN2*) transcripts in null mutant inflorescences binned in our experiments as early developmental pool (Figure 8B, see *OsGI* and *RCN2*). Functional characterization of these genes, employing the corresponding mutant or overexpression lines, demonstrated their roles in the control of flowering time or transition to flowering (Nakagawa et al., 2002; Hayama et al., 2003; Lee et al., 2012; Wu et al., 2018). We propose that low level expression of *OsMADS2* in vegetative SAM may mediate the activation of these genes to suppress precocious floral transition. The most striking floral phenotype in *osmads2* mutant is loss of lodicule identity and its abnormal development as organ with glume-like or mtp-like characteristics. In the transcriptome dataset from tissue pool termed in our experiments as middle stage (5-10 mm), notable are *PROTEIN TRANSPORTER 2* (*OsPTR2*, logFC = -0.914, FDR = 0.001), *HOMEOBOX GENE 1* (*HOX1*) and *ILA1 interacting proteins 3* (*IIP3*) (Figure 8C; Supplemental Dataset 2). Deregulation of their expression correlates with abnormal number and arrangement of vasculature in *osmads2* mutant lodicules, as their functions in vascular development are reported or speculated in several studies (Scarpella et al., 2000; Ning et al., 2011; Li et al., 2015). Of particular significance to cell wall thickening and lignification observed in *osmads2* mutant lodicules, our ontological analyses of DEGs indicated enrichment of cell wall GO term in the repressed gene subset (Fig 8A). Examples from this category are *PECTIN METHYLESTERASE 24* (*PME24*) and *BETA GLUCOSIDSE 30* (*BGLU30*). The higher expression level of *PME24* and *BGLU30* in mutant inflorescences in middle- and in all 3 stages, respectively (Figure 8, B-D; Supplementary Dataset 2) could alter cell wall mechanical flexibility and lignification as members of these gene families are reported to modulate cell wall composition in several studies (Hongo et al., 2012; Wang et al., 2013). Particularly, PMEs were shown to control pectin methylesterification activity in lodicules and regulate flower opening time, leading to the proposal that lower degree of pectin methylesterification in lodicules leads to cell wall rigidity and delays flower opening (Wang et al., 2022). Further, temporally staged flower

opening by osmosis-based dilation of lodicules has to be coordinated with stamen filament elongation and timed anther dehiscence. In this regard, several DEGs in *osmads2* mutant inflorescences have functions associated with osmotic homeostasis. Examples from this category are aquaporins such as *TONOPLAST INTRINSIC PROTEIN 4;3* (*TIP4-3*) and *PLASMA MEMBRANE INTRINSIC PROTEIN 2;6* (*PIP2-6*, Sakurai et al., 2005), and *OsTPKb*, encoding K^+ selective ion channel predominantly localized to the tonoplast of small vacuoles and is shown to confer osmotic tolerance in rice by Ahmed et al. (2016). Lodicule expansion is driven by the influx of water associated with the accumulation of K^+ and increased expression of aquaporins (Heslop-Harrison and Heslop-Harrison, 1996; Li et al., 2022). Hence, the lowered transcript levels of these genes in *osmads2* mutant inflorescence (Figure 8B for *OsTPKb* and Supplementary Dataset 2) may compromise the osmotic turgor of lodicules. Such defects may relate to fully closed florets we report in *osmads2 osmads4kd* plants. As per MSU database and our phylogenetic analysis of rice genome for MYB TFs (Supplemental Figure 12), we identified three rice *MIXTA-like* genes, two of them (OsMYB39 and Os02g0579300/LOC_Os02g36890) are regulated by OsMADS2 in the middle stage transcriptome (Figure 8B; Supplementary Dataset 2). We speculate these two rice genes may underlie the abnormal elongated epidermal cell fate in the *osmads2* transformed lodicules. This speculation is based on studies reporting regulation of petal and tepal epidermal cell development by *MIXTA-like* factors (Lu et al., 2022; Reed et al., 2022). We have shown by SEM that the distal overgrowth in elongated mutant lodicule is likely attributed to altered cell fate associated with increased cell division and cell expansion. Further, the increased number of floral organs in *omads2* and *osmads2 osmads4kd* florets suggests increased cell proliferation in the young floral meristems during organ primordia development as supported by increased floret meristem size (Supplementary Figure 8, G and H). Among DEGs which could contribute to increased cell proliferation and cell expansion phenotype in mutant *osmads2* developing florets are *FLORAL ORGAN NUMBER 1* (*FON1; CLVATA1 CLAVATA1* ortholog) and *WRKY24*. The former is a negative regulator of meristem size, and the latter is a positive regulator of cell elongation in rice (Suzaki et al., 2004; Jang et al., 2017). In 0.5 to 1 cm *osmads2* panicles with young FMs and early-stage organ primordia, *FON1* is downregulated while *WRKY24* is upregulated (Figure 8B; Supplementary dataset 2). This deregulation is together consistent with increased cell proliferation and meristem size in *osmads2* (Supplementary Figure 8G) and cell expansion in *osmads2* abnormal lodicule. Lodicule sections in *osmads2*$^{d8/d8}$ and *osmads2*$^{d8/d8}$ *osmads4kd* suggest decreased parenchyma cell layers across adaxial-abaxial axis. Candidate OsMADS2 downstream target that could underlie this

phenotype is *RICE SQUAMOSA PROMOTER-BINDING-LIKE 16* (*SPL16*). This gene is a positive regulator of cell division (Wang et al., 2012) and is downregulated in *osmads2*$^{d8/d8}$ 0.5-1 cm inflorescences (Fig 8C; Supplementary dataset 2). Consistent with conserved functions for a B-class factor OsMADS2, downstream targets include several genes implicated for anther/pollen development. Examples from this category of OsMADS2 regulated targets are *CARBON STARVED ANTHER* (*CSA*), *MICROSPORELESS1* (*MIL1*), *TAPETUM DEGENERATION RETARDATION* (*TDR*), *SPOROCYTELESS* (*SPL*), *GERM CELL SPECIFIC 1 (GCS1)* and *MICROSPORE AND TAPETUM REGULATOR1* (*MTR1*) (Li et al., 2006; Zhang et al., 2010; Hong et al., 2012; Tan et al., 2012; Ren et al., 2018; Honma et al., 2020). These genes are downregulated in *osmads2* inflorescence in either or both middle and late stages (Figure 8, B and C; Supplementary dataset 2). Although gross stamen morphology was apparently normal in *osmads2* single mutant, the additional disruption by RNAi of *OsMADS4* in *osmads2* background rendered these double mutant plants sterile. Interestingly, *osmads2* mutant exhibited reduced expression of *LONG STERILE LEMMAS 1* (*G1*), *NONSTOP GLUMES 1* (*NSG1*) and *DEPRESSED PALEA 1*/*DP1* (Fig 8B; Supplementary dataset 2) which regulate SL specification (Yoshida et al., 2009; Jin et al., 2011; Xu et al., 2020). Since rice *PISTILLATA* paralogs are not detectably expressed in the SL (Kyozuka et al., 2000; Yadav et al., 2007), the abnormal SL phenotype in *osmads2* and *osmads2 osmads4kd* plants suggests the roles of these genes in SL specification, is perhaps redundant with other genes, or that their action in SL might be non-cell-autonomous. Alternatively, a relatively low expression of rice *PISTILLATA* in SL that is not detected by RNA *in situ* hybridization may be contributing to normal development of SL. The latter hypothesis is supported by the reported expression of rice *PISTILLATA* in SL gene expression cluster as detected by single cell transcriptome (Zong et al., 2022). Future studies with higher order mutants with *g1*, *nsg1*, *dp1* and *osmads2* in genetic interaction studies would aid the indications from our study. Rachis elongation in rice aids panicle exertion for proper seed setting post fertilization. Although *osmads2* single mutant and *osmads4kd* plants displayed apparently normal panicle booting, combined disruption of both *PI* paralogs severely compromised this process. Examples of OsMADS2 regulated DEGs that could contribute to this process are GA biosynthetic genes *GA20OX2/SEMIDWARF 1* and *OsGA3ox2/d8*, both of which are downregulated in 0.5-1 cm *osmads2* inflorescence tissues (Figure 8B; Supplementary dataset 2). Interestingly, *EPIGENETIC SHORT PAICLE* (*ESP*) encoding a long noncoding RNA was consistently upregulated across the three developmental tissue pools studied here (Figure 8B). This is another candidate downstream target of OsMADS2 that can underlie the enclosed panicle

phenotype since a gain-of-function epiallele of *ESP* is reported to have short panicles (Luan et al., 2019). The similarity between *osmads2* and *osmads32* phenotypes with respect to lodicule identity transformation, formation of ectopic lodicules and chimeric floral organs prompted us to ask whether these MADS factors regulate each other. Importantly, while the interaction of OsMADS32 with rice PISTILLATA was shown by yeast 2 hybrid assay (Wang et al. 2015), the expression levels of the rice *PI* orthologs are not affected in *cfo1*-2 (Hu et al. 2021). Also, we find the expression of *OsMADS32* was not significantly altered in *osmads2*$^{d8/d8}$ mutant. These observations together suggest that OsMADS2, OsMADS4 and OsMADS32 perhaps cooperate (as a complex) to regulate other genes without transcriptional feedback among themselves. Overall, these results highlight the molecular functions of OsMADS2 in rice floral organ development and further provide leads on unique evolved roles in rachis elongation, floral meristem size and floral organ number. The distinct roles of OsMADS2, as compared to *AtPI*, suggest significant change in their downstream targets. We compared the differentially expressed gene sets of *pi-1* (Wuest et al., 2012) with that in *osmads2*$^{d8/d8}$ of our study. Interestingly, in *pi-1*, the number of DEGs increased with the progress of flower development. To some extent, we observed similar trend in rice inflorescence tissues pooled as per study, specifically when we compare early and middle stage. However, in our tissue sample termed late stage (1-2 cm panicles), the number of DEGs are much reduced. Unlike *osmads2*$^{d8/d8}$ where majority of DEGs were downregulated, indicate an overall transcription activation role for this rice factor, the downstream gene sets regulated by PI include nearly equal numbers both positively and negatively deregulated genes. Orthologs group analysis indicated that nearly 15% of *OsMADS2* downstream targets have orthologs deregulated in at least one floral developmental stage of *Arabidopsis pi-1* mutant (Supplementary Dataset 4). Interestingly among rice genes downstream targets of OsMADS2 that have *Arabidopsis* orthologs regulated by AtPI are *RCN2*, *OsHOX1*, *CSA*, *GCS1* and *BHLH120*. *RCN2* is downregulated in *osmads2*$^{d8/d8}$ early stage (0.2-0.5 cm inflorescence pool) which may be underlying the early flowering phenotype seen in these plants. However, in slightly later stage (0.5-1 cm inflorescence pool), *RCN2* is upregulated. Similarly, its *Arabidopsis* ortholog *TFL1* is upregulated in stage 3-4 (corresponding to 2.5 days after induction of *Arabidopsis* flower formation). This increased expression in a relatively later stages suggests these orthologs, as common downstream targets of both OsMADS2 and PI, rather conserved for the control of floral meristem identity not flowering time. *BHLH120* and its *Arabidopsis* orthologs *HEC1* and *HEC2* were upregulated in *osmads2*$^{d8/d8}$ and *pi-1* DEG datasets suggesting that suppression of regulators of carpel development by B-function genes may be evolutionary conserved.

Remarkably, several TCP transcription factors downstream of OsMADS2 had their orthologs represented in *pi-1* DEG dataset. Examples are *OsPCF1*, *OsPCF5*, *OsTCP9*, *OsTCP21*. Notably *osmads2* downstream targets regulating flowering time such *OsGI* and *OsMADS55* were not reported in the *pi-1* DEG dataset. Also, auxin biosynthetic genes *OsYUC3* and *OsYUC7* that are downstream targets of OsMADS2 are not represented in *pi-1* dataset. Together, these bioinformatic analysis of the expression levels of predicted orthologous genes between *Arabidopsis* and rice provide clues to some evolutionary evolved functions of *OsMADS2* as compared to *AtPI*.

Inference of Gene Regulatory Network acting downstream to OsMADS2

The transcriptome datasets and the ChIP-Seq dataset were utilized to construct OsMADS2 GRN. To identify *OsMADS2* directly regulated genes, we overlapped the 2,589 OsMADS2 bound genes (ChIP-Seq output) with the DEGs (RNA-Seq output) from the three stages. For this analysis we considered DEGs with 1.5-fold change and qvalue ≤ 0.05. Genes common to both datasets (ChIP-Seq and RNA-Seq) were designated as OsMADS2 potential direct targets. Interestingly, ~ 18% of the bound genes were deregulated in at least one of the three stages with middle stage sharing the most OsMADS2 bound genes (Figure 9A). Two predicted GRNs were generated for OsMADS2 downstream targets deregulated in 0.2-0.5 cm inflorescence and 0.5-1 cm inflorescence. Transcription factors that are bound and regulated by OsMADS2 were used as main nodal genes in the GRN. Assumed promotor sequences (-100 to 500 from TSS) of OsMADS2 downstream targets were searched for occurrences of DNA binding motifs for these transcription factors. OsMADS2 binding and regulation of certain nodes from the GRN was validated by ChIP-qPCR and RT-qPCR (Figure 7 and Figure 8). In early-stage inflorescences (0.2-0.5 cm) majority of OsMADS2 indirect targets were linked to the nodes of HSFC1B and WRKY8, while for middle stage GRN (0.5-1 cm inflorescence), ARF7A, HSFC1B, PCF2 and PCF5 linked out majority of OsMADS2 indirect targets (Figure 9B; Supplemental Figure 15; Supplementary Dataset 5).

Discussion

In this study, we elucidate the roles of *OsMADS2* and its paralogous gene *OsMADS4* in rice floral development. We showed that *osmads2* null mutant bear abnormal lodicule and unaffected stamens, reiterating on the unique sub-functionalization of *OsMADS2* in lodicule development. We presented evidences that sub-functionalized rice *PI-like* paralogs likely

encode equivalent proteins, suggesting that the acquired nonredundant role of *OsMADS2* in lodicule arise, largely, from divergence in the *cis* DNA elements that drive its expression. Further, we presented evidences for distinct roles of rice *PI-like* factors in regulating flowering time, floral organ number, and in suppressing parthenocarpy. Importantly, we uncovered OsMADS2 gene targets by which it can execute specific floral organ differentiation programs. We showed that genome edited null mutants in *OsMADS2* bear florets with partial homeotic transformation of lodicule to abnormally elongated flattened organs that have mosaic cellular differentiation patterns. We gained insights into the identity of the homeotic transformed organs by careful examination of external cell morphologies and internal cellular characteristics and their spatial distribution along proximo-distal and ab-adaxial axes. The SEM micrographs indicate that *osmads2* florets cells, along the proximal–distal axis of the abnormal lodicules, are committed to different fates. In these abnormal lodicules, elongated epidermal cells seen at the distal end and at regions abutting the palea (marginal tissue of palea: MTP) suggested partial homeotic transformation of the lodicules to tissues representing an adjacent organ. Other more severe phenotypes in *osmads2* florets were increased organ numbers, also seen in the maize *Zmm16*/*sterile tassel silky ear1* mutant but not in *Arabidopsis pi-1* mutant (Bowman et al., 1989; Yang et al., 2003; Bartlett et al., 2015). The generation of ectopic lodicules on opposing side, underlying the palea, indicates restoration of a full second whorl primordia. This shows a role of *OsMADS2* in mediating normal lodicule position asymmetry, *i.e.*, 2 lodicules in half whorl configuration, which we suggest could arise by controlling local auxin maxima. Other abnormalities in *osmads2* include florets with an excess of carpels (partial *superwomen*) and presence of chimeric organs. These stronger phenotypes could arise from a near complete loss of B-class activity due to reduced or late onset of *OsMADS4* expression or to high temperature (un-favoring the OsMADS4-SPW1 dimer formation, Yoshida *et al.* (2007)). In support of this hypothesis, it has been reported that *DROPPING LEAF* (*DL*) and both floral organ patterning class C MADS genes; *OsMADS3/58*, are misexpressed in whorl 2 organs of *OsMADS2* RNAi transgenics and in *OsMADS2* RNAi + *OsMADS4* RNAi double knockdown transgenics, but plants with *OsMADS4* RNAi alone (Yao et al., 2008). Hence, suggesting a compromised class B activity that is required to antagonize the expression of *DL* and C-class genes in whorl 2.

Although *osmads4kd* floral organs were normal, disruption of *OsMADS4* in *osmads2* mutant further augmented its abnormality. In the double mutant, florets exhibited nearly complete transformation of the lodicule to glume or palea-like organs as indicated by increased

lignification, development of midrib vein and bubble-shaped cells lining the adaxial side of these abnormal transformed lodicules. These results confirm the redundant role of *OsMADS4* with regard to lodicule development. Although some early insights on genetic redundancy of rice *PI* paralogs with regard to lodicule development were reported by RNAi single and double knockdown (KD) studies of Yao et al., (2008), the double KD plants in this study were sterile and could not be advanced in generations for careful phenotyping and transcriptomic analyses. Hence, our approach of developing simultaneous disruption by crossing *osmads2* with *OsMADS4 dsRNAi* enables generation of stable and fertile *osmads2*$^{+/-}$ *OsMADS4 dsRNAi* transgenics that could be advanced in generations and yield segregants that are doubly mutant: *osmads2*$^{-/-}$ *OsMADS4 dsRNAi* for careful phenotypic comparisons with WT and heterozygous siblings. On these plants, we clearly identified phenotypes, not reported in the single mutant parents of the cross, that arise only in double mutant segregants. As seen in Zhao et al. (2022), stamen filaments failed to elongate in the unopened *osmads2*$^{d8/d8}$ *osmads4kd* florets. This suggest that the timely coordinated floret opening and stamen filament elongation processes are both controlled by common triggers for water influx and cell elongation. The accumulation of potassium ion in cells is one of these triggers (Heslop-Harrison and Heslop-Harrison, 1996). Unlike rice *PI-like* genes, maize, *PI* paralog; *Zmm16/sts1* exhibits no redundancy with paralogous *Zmm18/29,* as *sts1* mutants had a homeotic conversion of second whorl lodicules and third whorl stamens into lemmas/paleae. This incongruity in functions between rice and maize *PI* paralog was hypothesized to be attributed to either incomplete silencing of *PI* paralogs in rice or lack of organ-specific expression sub-functionalization in maize (Bartlett et al., 2015). Here, in our study, using a null *osmads2* mutant, we showed that stamens are not affected, demonstrating a complete redundancy rice *PI* paralogs in stamen and suggesting that the third whorl phenotype seen in maize *sts1* mutant is likely attributed to lack of organ-specific expression sub-functionalization of maize *PI* paralogs. We provided leads that also favour the underlying molecular mechanism as sub-functionalization of rice *PI* paralogs based on detailed observations from our complementation analysis (Figure 1F). Notably, ubiquitous overexpression of *OsMADS4* in *osmads2* rescued the lodicule abnormality suggesting that the functional divergence, seen on individual loss of function mutants/knockdowns, most likely arises from their spatio-temporal expression pattern and/or relative expression levels. This possibility is consistent with the variations in their spatial expression patterns and abundance as seen in RNA *in situ* hybridization (Yadav et al., 2007) and from our NGS analyses (Supplemental Figure 5D; Supplemental Figure 11E). Apparently, rice *PI* paralogs have an additional redundant role in the control of cell proliferation as demonstrated from the increased

meristem size and floral organ number in *osmads2*$^{-/-}$ single mutant and *osmads2*$^{-/-}$ *osmads4kd* transgenics. Further, the undifferentiation and excess growth of ovules/nucellar tissue in the double mutant also reveals that there is an increased whorl-specific proliferation even in the fourth whorl though *OsMADS2* transcript is absent (Yadav et al., 2007). A likely mechanism by which rice *PI* paralogs impact fourth whorl is probably by control of local changes in auxin levels. We hypothesize that in *osmads2 osmads4kd*, increased third whorl auxin level is polarly transported to fourth whorl to promote nucellar proliferation.

The identity of floral organs is dictated by combinatory functions of different classes of transcription factors (Coen and Meyerowitz, 1991; Pinyopich et al., 2003; Favaro et al., 2003). In *Arabidopsis*, although ectopic expression of *PI* or *AP3* alone did not significantly alter flower development, their simultaneous ectopic expression converted sepals to petals, and carpels to stamens (Krizek and Meyerowitz, 1996). In rice, ectopic overexpression of *OsMADS16* enhanced *OsMADS4* expression and produced multiple stamen-like structures in the innermost whorl (Lee et al., 2003). Interestingly, in our study, we found that neither ubiquitous overexpression of *AtPI* in WT rice, nor overexpression of *OsMADS4* in *osmads2* results in homeotic alteration of floral organs. These results indicate that coexistence of PI and AP3 protein homologs, in reasonable levels, as a prerequisite for ectopic B-class activity is conserved in rice. Interestingly, we have shown that ubiquitous overexpression of *PI-like* genes in rice resulted in the formation of underdeveloped stamens, a phenotype which was also reported in *OsMADS16* overexpression rice lines but not reported for *PI* or *AP3* when overexpressed in *Arabidopsis* (Jack et al.; 1994; Krizek and Meyerowitz, 1996; Lee et al., 2003). These together suggest that excess constitutive and ubiquitous B-class activity is detrimental for normal anther development. Intriguingly, at low penetrance in rice *PI-OX* line there is an increased stamen number similar to that commonly seen effect of *OsMADS16* and *AP3* overexpression in rice and *Arabidopsis*, respectively (Jack et al.; 1994; Lee et al., 2003). Together these results exemplify cases of conservation and divergence of the B-class genes within rice and between rice and *Arabidopsis*. Gene duplication may allow compensation of phenotypic errors attributed to genotypic or phenotypic mutations or attributed to stochastic fluctuations in gene expression (Elowitz et al., 2002; Balázsi et al., 2011). In rice, *PI*-lineage is an example for where duplicated genes allow each paralog to contribute to phenotypic error buffering. The loss of this error buffering can explain the low penetrance phenotypes such as lodicule-stamen, stamen-carpel chimeric organs and partial superwoman observed in *osmads2* single mutant. The fact that neither *OsMADS4, OsMADS16, OsMADS32* or *DROOPING LEAF*

(*DL*) were significantly deregulated in *osmads2* make us propose that such very infrequent phenotypes can be due to stochastic fluctuations in gene expression.

Understanding the mechanism of lodicules function and development is important for breeders to develop cleistogamous and early floret opening time (EFOT) lines. Work done by Yoshida et al. (2007) showed that a missense mutation in *OsMADS16/SPW1* could generate cleistogamous plants with normal stamens. Here we found that simultaneous disruption of rice *PI* orthologs, in *osmads2*$^{d8/d8}$ *osmads4kd* double mutant, fully abolishes floret opening. Unfortunately, these unopened florets were sterile. One strategy to develop cleistogamous rice is by utilizing lodicules specific *cis* acting promotors to express dsRNAi against *OsMADS4* in *osmads2* mutant background. This strategy will be feasible upon identification of lodicule-specific *cis* elements in the future. On the other hand, EFOT rice lines are required to mitigate the heat-induced floret sterility. OsMADS2 targets *PME24* and *BGLU30* are candidates of lodicules cell wall metabolism genes that can be engineered to influence floret opening time, as shown for *PME40, PME42* and *BETA-1,3-GLUCANASE 4* (*GNS4*) in rice (Wang et al., 2022; Xu et al., 2022).

The onset of normal fruit development depends on successful fertilization. However, in parthenocarpy, fruit formation from maternal tissue can be triggered without fertilization. Although recognized as an important trait to counter harsh environmental conditions and produce seedless fruits that are preferred by consumers, this process however adversely affects biodiversity. Hence, plants have evolved several mechanisms by which they can counter or trigger this process (Reviewed in Joldersma and Liu, 2018), however in rice information on these mechanisms are scarce. In rice, parthenocarpy was shown to be triggered by auxin application *in vitro* from dissected unfertilized rice spikelets and *in planta* (Uchiumi and Okamoto 2010; Zhao et al., 2013). Here we have shown that rice *PISTILLATA* paralogs redundantly mediate the suppression of parthenocarpy. The increased FM size, floral organ number and the undifferentiated nucellar masses seen in *osmads2* and *osmads2 osmads4kd* florets, together suggest that the double mutant florets may have elevated auxin level by which parthenocarpy is triggered. Unsurprisingly, the transcriptomic analysis demonstrated deregulation of some known auxin biosynthetic genes; *OsYUCCA3* and *OsYUCCA7* with elevated expression in *osmads2* mutant panicle tissues. Importantly, the transcriptomic data also uncovered several *OsMADS2* target genes whose functions are linked to the various floral abnormalities found in *osmads2* mutant. Remarkable, is the deregulation of abiotic stress tolerance and cell wall organization genes. Modulation of cell wall metabolism and osmotic

responses are strongly linked as indicated from different omics data (Reviewed in Veronico et al., 2022). In context of lodicules, this modulation is required to facilitate its dilation and shrinking during anthesis and post anthesis, respectively.

In conclusion, the *osmads2* generated in this study gives new insights on the role of *OsMADS2* in rice floral development. Importantly, *osmads2;* the stable and fertile mutant allele served as a source to create higher order mutant; *osmads2 osmads4kd* which can be maintained as heterozygous. This line, together with *osmads2* single mutant will serve to create additional higher order mutants and strains to probe the contribution of key nodal downstream targets of *OsMADS2* and *OsMADS4* that control spatial tissue differentiation in floral organs.

Materials and Methods

Plasmid construction and plant transformation

For CRISPR/Cas9 genome editing of *OsMADS2*, two pairs of primers were designed for respective sets of 20 nucleotides guide RNA (gRNA). The first pair of primers (a and b) were annealed and cloned into the commercial pRGEB31 vector to construct a binary vector used to raise transgenic plants with intended editing in OsMADS2 DNA binding domain (Designated as gRNA1). The second pair of primers (c and d) were annealed and cloned similarly and the construct was used to raise transgenic plants with intended editing in OsMADS2 K-Domain (Designated as gRNA2). The sequences for the different oligos are given in Supplemental Data Table S3. For *OsMADS4* dsRNAi based knockdown, a 290 bp specific fragment (from +1794 to +2083 of OsMADS4 genomic locus was amplified using *OsMADS4* FP and *OsMADS4* RP primers (Supplemental Data Table S3). This fragment was then cloned into pBluescript in opposite orientations separated by stuffer. The generated clone was verified by restriction digestion and Sanger sequencing. Subsequently, the insert in recombinant pBluescript was released and cloned in the binary rice expression vector pUN (Prasad et al., 2001) downstream to the maize ubiquitin promoter for expression of OsMADS4 hairpin. For overexpression of *OsMADS4* in *osmads2* mutant background, *OsMADS4* cDNA was amplified with OsMADS4 CDS FP and RP (Supplemental Data Table S3), from cDNA library prepared from TP309 panicle tissues and cloned into pBluescript. A clone verified by restriction digestion and Sanger sequencing was used to released OsMADS4 cDNA which was subsequently cloned downstream to maize ubiquitin promoter into a modified pCAMBIA3300 (has ZmpUbiq promotor and Nos terminator). This basta resistant vector was used to transform rice calli

generated from mature seeds from *osmads2* mutant. For overexpression of *Pistillata* in WT rice, full-length cDNA was PCR amplified from pBS-PI vector (from Prof. Meyerowitz lab) using PI FP and PI RP primers to introduce BamHI and KpnI at the 5' and 3' ends, respectively (Supplemental Data Table S3). The PCR amplicon was cloned in pBluescript. Subsequently the cDNA was released from a clone verified by restriction digestion and Sanger sequencing and ligated in pUN (Prasad et al., 2001) downstream to maize ubiquitin promotor. Unless mentioned otherwise, binary vectors were mobilized into LBA4404 *Agrobacterium tumefaciens* strain which was used to transform WT rice (*Oryza sativa* var. Japonica) TP309 embryogenic calli and raising transgenic lines as described by Prasad et al. (2001). Transgenic plants, grown in IISc, Bangalore, Green house condition, ~27°C always along with wild-type controls. For raising anti-OsMADS2 antibody, a gene-specific *OsMADS2* cDNA fragment encoding amino acids 112 to 209 was cloned in pET-15b and the His-tagged protein was expressed in bacterial culture grown with 0.5 mm isopropylthio-β-galactoside at 37°C for 3 hours. The His-tagged OsMADS2 partial protein was purified by nickel-nitrilotriacetic acid agarose chromatography and then the His tags were removed by thrombin cleavage. The purified proteins were used to raise rabbit polyclonal antibodies that were antigen affinity purified. Specificity of the purified antibody was established by western blot on nuclear protein from panicle.

Genotyping of CRISPR/Cas9 edited *OsMADS2* lines

Genomic DNA region flanking the editing sites was PCR amplified using OsMADS2 E3-I3 FP and OsMADS2 IV RP (Supplemental Data Table S3). PCR amplicon was digested with SacI to identify *OsMADS2* putatively edited plants. Subsequently, PCR amplicon from putatively edited plants was cloned in EcoRV site of pBluescript and at least two pBSKS clones were given for Sanger sequencing to identify the exact editing. To identify plants with germlines inherited mutant alleles, independent genotyping was done from two subsequent leaves from same plant and across different generations. Once mutant plants with stable germline inherited alleles were identified, Sanger sequencing of PCR products was utilized for further genotyping in advanced generations.

Amplifying the genomic DNA flanking the T-DNA integration site

Restriction Site Extension PCR (Ji and Braam, 2010) was utilized to amplify the genomic DNA flanking the T-DNA harbouring *OsMADS4* dsRNAi cassette. Briefly, p1300 5.0 and p1300 5.1; two primers specific to pCAMBIA1300 left border (Supplemental Data Table S3) were

used to perform the primary and secondary PCRs, respectively. Two amplicons of ~ 1.2 and ~ 1.4 were obtained from genomic DNA digested with SacI and KpnI, respectively. These amplicons were gel-purified and sequenced. The genomic sequence flanking the T-DNA left border was then mapped to rice genome using blastn. To screen transgenic plants for zygosity with respect to *OsMADS4* dsRNAi cassette integration, two primers (OsM4 ds IS FP and RP) flanking both sides of the insertion site were designed and utilized to amplify WT genomic sequence from hemizygous and azygous segregants.

Phenotypic Characterization

Freshly collected pre-anthesis mature spikelets (Itoh et al., 2005) were examined and photographed using a Leica Wild M3Z stereomicroscope fitted with digital camera (Canon Powershot G5). Pollen from rice anther in S13-S14 (Zhang et al., 2011) stages were stained with either Iodine Potassium Iodide (I2KI) or 4′,6-diamidino-2-phenylindole (DAPI) for 1-5 mine on a microscope slide and examined by microscope. Phenotyping of ovaries and ovules by whole-mount eosin B-staining confocal laser scanning microscopy was according to Zeng et al. (2007). For SEM, fresh spikelet and inflorescence samples were fixed in 0.1 M sodium phosphate buffer pH 7.0 containing 3% glutraldehyde (Sigma-Aldrich, St. Louis, USA) for 12-24 hr. The tissue samples were then post fixed in 1% osmium tetroxide for 24-48 hr or until performing the next step. Next, tissue samples undergone graded ethanol dehydration and then critical point dried using Pelco CPD2. Critical point dried tissue samples were then mounted on the SEM stub using double stick conductive carbon tape, sputter coated and examined. Ultra 55 FE-SEM with EDS (Carl Zeiss) instrument was used for imaging with help from the technical person in charge at Centre for Nano Science and Engineering (CeNSE), IISc. For histological analysis, tissues were fixed in FAA solution, dehydrated in ethanol series and embedded in paraffin. Sections of 8 um were stained with 0.5% Toluidene Blue.

Western Blot

Nuclear protein was isolated according to Busk and Pages (1997). Protein concentration was estimated by Bradford method according to the manufacturer’s instructions. The protein was separated on SDS PAGE gel of 12% and transferred to PVDF membrane of 0.5 µm pores through semidry transblot (Biorad). Blocking was then done for 1hr followed by primary antibody (polyclonal affinity purified primary antibody against 14 KD C-terminal region of OsMADS2) for 12 hrs. Washing was then done for 5 min 3X and then the membrane was

incubated with the HRP conjugated secondary antibody for 1 hr. washing was then done 3X for 5 minutes each and developed using Immobilon Forte Western HRP Substrate (Cat# WBLUF0100). Images were acquired using ImageQuant LAS4000 Chemidoc instrument of MCB, IISC.

ChIP-sequencing, alignment, peak calling and gene assignment

Wild-type TP309 panicles of 0.3-2 cm size (~200mg) were used for the ChIP. The tissues were fixed with 1% formaldehyde in fixation buffer. OsMADS2 ChIP was performed using SimpleChIP® Enzymatic Chromatin IP Kit (Cat #9002, CST). MNaseI based chromatin was prepared with DNA size range of 150bp to 900bp. For the ChIP, 8µg of chromatin was taken and incubated with 6µg of antigen-affinity purified anti-OsMADS2 antibody. The DNA-protein complexes were pulled down using protein-A magnetic beads. Simultaneously a negative control sample using rabbit IgG antibody (Mock IP) instead of the anti-OsMADS2 antibody was processed similarly. Immunoprecipitated DNA was eluted using elution buffer provided in the kit and reverse cross-linked using 2M RNase A, 4M proteinase K and 5M NaCl for 6 hours at 65˚C. Reverse-crosslinked ChIP DNA was purified using phenol/chloroform precipitation method. Approximately 6ng of ChIP DNA was processed for library preparation for Next Generation Sequencing by using Kapa kit (Roche) following the manufacturer's instruction with one modification, as we performed the library amplification before the double-size selection. The NGS was performed using Illumina HiSeq2500 machine. Raw fastq files were processed with FASTQC and Fastp for filtering low quality reads and adaptor trimming. Next, Short read alignment was performed by bowtie2 version 2.3.5.1 using MSU-TIGR v7 as reference genome. The bam files with alignment information were process with SAMBAMBA (0.6.6) for sorting and filtering uniquely mapped reads. For peak calling, the uniquely mapped reads were processed with MACS2 (2.2.6, Zhang et al., 2008) with default parameters, keep-dup parameter as AUTO and effective genome size of 3.50e+08. Briefly, two biological replicates (B5 & B6) of IP and Mock-IP were used. First, peaks from IP B5 were retrieved using Mock-IP B5 as control. Another set of peaks from IP B5 were retrieved using Mock-IP B6 as control. Next, peaks from IP B6 were recovered using Mock-IP B6 as control. To determine confident peaks from B5 IP, overlapped peaks from its two sets were recovered and merged. These confident peaks from IP B5 were then merged with overlapped peaks from IP B6. These overlapped merged peaks from IP B5 and IP B6 were designated as confident peaks. Next, the confident peaks were assigned to genes in their neighbourhood up to 4000 bp from either the start or end of the gene. Finding overlapped peaks and peak merging was performed

in R studio using findOverlapsOfPeaks () function from ChIPpeakAnno Bioconductor package with default parameters. Peaks assignment to genes was done with annoPeaks () function from ChIPpeakAnno Bioconductor package (Zhu et al., 2010) with bindingType set as "fullRange" and bindingRegion set as -4000 and 4000. Peak distribution with respect to TSS and 3000 bp flanks was performed with plotAvgProf () from ChIPseeker Bioconductor package (Yu et all., 2015) using coordinates from "Oryza_sativa.IRGSP-1.0.53.gtf.gz".

ChIP-Seq motif analyses

Coordinates of the confident peaks were defined from IP B5. The midpoints of these peaks were determined and a set of 500 bp (-250 to 249 from the midpoints) sequences was extracted. In these 500 bp sequences, the repeats were masked using RepeatMasker (https://www.repeatmasker.org/) and then submitted to MEME-ChIP from MEME suite (Machanick and Bailey, 2011). From MEME analyses we retrieved significantly enriched motifs with E value <= 0.05. For plotting motif enrichment in peak region and flanking 3000 bp in 400 bp windows, we utilized a house built-in R script using vmatchPattern () function from Biostrings Bioconductor package (Pagès et al., 2022).

RNA-Sequencing and orthologous group analysis

RNA-sequencing of WT and *osmads2*$^{d8/d8}$ was done for three and two biological replicates, respectively. First, total RNA was extracted from panicle tissue by TRIzol R reagents (Invitrogen, Carlsbad, CA, United States). RNA was then treated with DNAse I (Promega) to remove gDNA contaminant according to manufacturer's protocol. Further, RNA quality and concentration was examined by Agilent TapeStation and Qubit, respectively. RNA of integrity number (RIN) > 7 was used for library construction. Total RNA of 500 ng was used to enrich the mRNA using NEBNext Poly (A) mRNA magnetic isolation module (Catalog: E7490, New England Biolabs) by following the manufacturers' protocol. The enriched mRNAs were further taken for the library preparation using the NEBNext® Ultra™ II RNA Library Prep Kit for Illumina (Catalog: E7775S, New England Biolabs). Sequence data was generated using Illumina HiSeq, pair-end 2X150bp chemistry. Data was checked for base call quality distribution, percentage of bases above Q20, Q30, %GC, and sequencing adapter contamination using FastQC and MultiQC software. All the samples have passed QC threshold (Q30>90%). Further, raw sequence reads were processed to remove adapter sequences and low-quality bases using fastp. The QC passed reads were then mapped onto indexed *Oryza sativa* ssp. japonica cv. reference genome (RAP-DB; https://rapdb.dna.affrc.go.jp/) using STAR v2 aligner. On average, 99.9% of the reads aligned to the reference genome. Raw reads

were counted with featureCounts function from Rsubread package. Differential expression analysis was carried out using the edgeR package after normalizing the read counts based on trimmed mean of M (TMM) values. Replicates from *osmads2*$^{d8d/d8}$ was compared to replicates from WT. Genes with absolute log2 fold change ≥ 1 and adjusted p-value ≤ 0.05 were considered significant. The raw data of available RNA-Seq dataset for shoot apical meristem in rice; GSE90493; GSM2402820; SRR5052708 and GSM2402821; SRR5052708 (Gómez-Ariza et al., 2019) were downloaded from NCBI and mapping was performed as described above. The raw data of available RNA-Seq dataset for shoot apical meristem in Arabidopsis; PRJNA268115; SRR2073174 (Klepikova et al., 2015) was downloaded from NCBI and mapped to TAIR9 Genome Release. For orthologous group analysis, list of orthologous groups (file name: APK_ftp_file.txt) was downloaded from Rice Genome Annotation Project (http://rice.uga.edu/annotation_pseudo_apk.shtml). This list was reorganized to contains only rice genes with corresponding Arabidopsis orthologs and then downsized to only those rice genes that are deregulated in at least one stage. This list was then overlapped with *pi-1* dataset to identify the rice genes downstream targets of OsMADS2 that have their orthologs represented in *pi-1* dataset of deregulated genes.

RT-qPCR and ChIP-qPCR

For RT-qPCR, oligo(dT) primed cDNAs were synthesized from total RNA with MMLV (reverse transcriptase, NEB). Reactions of qRT-PCR were set up with 50-70ng of cDNA and 250 nM gene-specific primers using FastStart Universal Sybr Green Master (Rox) mix (Roche). Fold change in transcript levels for deregulated genes was calculated as follows: ΔCt value was obtained by subtracting the Ct value for internal control, Ubiquitin5 from the Ct value for each gene of interest (Gene Ct-Ubi5 Ct). Next, ΔΔCt was calculated by subtracting ΔCt value for WT from the ΔCt value obtained for transgenic tissue. The fold change was calculated as 2^-(ΔΔCt). Primers used and their sequences are given in Supplemental Data Table S3. For ChIP-qPCR, Wild-type TP309 panicles of length 0.5-1 cm or 1-2 cm (~200mg) were used. The tissues were fixed with 1% formaldehyde in fixation buffer. OsMADS2 ChIP was performed using SimpleChIP® Enzymatic Chromatin IP Kit (Cat #9002, CST). MNaseI based chromatin was prepared with DNA size range of 150bp to 900bp. For the ChIP, 2 ul were kept as input for input DNA and 90 ul of chromatin was taken and incubated with 6µg of affinity purified anti-OsMADS2 antibody overnight. The DNA-protein complexes were pulled down using protein-A magnetic beads. Simultaneously a negative control sample (Mock IP, no antibody) was processed similarly. Immunoprecipitated DNA was eluted using elution buffer provided

in the kit and reverse cross-linked using 2M RNase A, 4M proteinase K and 5M NaCl for 6 hours at 65˚C. The DNA was then purified using column purification. For ChIP-qPCR, the final ChIP DNA was diluted 10 times and 1 µ used for qPCR with locus-specific primers (Appendix D). For each tested locus, two regions (peak and nonpeak) were amplified using DNA from input, IP and mock samples. First % Input was calculated as follows: %input for IP samples= 2^(CT.in-log2(DF)-CT.ip) and %input for Mock samples= 2^(CT.in-log2(DF)-CT.mock). CT.in, CT.ip and CT.mock refer to the average CT value for input, IP and mock samples respectively. DF refers to the dilution factor of the input. The relative enrichment was then calculated by dividing the %input in the peak region to %input in the nonpeak region. Hence, the values for the nonpeak regions were all set to 1. The data were derived from two independent replicates of OsMADS2 ChIP DNA along with respective Mock.

Inference of Gene Regulatory Network

We overlapped OsMADS2 bound genes (ChIP-Seq output) with the DEGs (RNA-Seq output) from the three progressive inflorescence stages to identify the direct target genes. Transcription factors from these direct target genes were extracted and used as first layer nodal genes to link OsMADS2 regulation to its downstream indirectly regulated genes. For this, promotor analysis was conducted to identify indirect targets with at least single occurrence of DNA binding motifs for WRKY8 (TTGACY), ERF65 (AGCCGCC), OsHOX2 (CAAT(G/C)ATTG), OsHOX4 (CAAT(T/A)ATTG), OsARF7A (TGTCTC), OsPCF2 (GGNCCCAC), OsPCF5 (GTGGNCCC), OsSPL2 (TNCGTACAA) and HSFC1B (TTCTAGAA/GAANNTTC). Occurrences of these motifs were checked in 600 bp assumed promotor sequence (-500 to +100 bp with respect to TSS). The binding site information were retrieved from PlantPAN3.0 database (Chow et.al., 2019).

Statistical Analysis

Chi-square test and P value of all statistical analyses was inferred using GraphPad Prism8 (Unpaired t test with Welch's correction and without assumption of equal SDs). Number of individuals and replicates is indicated separately for each experiment either at the figures or at the materials and methods section for each experiment.

Supplemental data

Supplemental Figure S1. Generation and characterization of CRISPR/Cas9-mediated *osmads2* heritable mutant alleles.

Supplemental Figure S2. Supporting phenotypic analysis of different generated genotypes studied.

Supplemental Figure S3. Supporting histological analysis of floral organs in different generated genotypes studied.

Supplemental Figure S4. Analysis of pollen viability in different genotypes studied.

Supplemental Figure S5. Analysis of flowering time in different generated genotypes studied and expression of MADS domain B class genes in shoot apical meristems.

Supplemental Figure S6. Analysis of B-class genes *OsMADS2* and *OsMADS4* fold change regulation in *osmads4kd#1* transgenics.

Supplemental Figure S7. Characterization of integration site and illustration of genotyping for zygosity of *OsMADS4* dsRNAi cassette.

Supplemental Figure S8. Scanning electron micrographs (SEM) in WT and rice *pistillata* mutants.

Supplemental Figure S9. Supporting histological analyses for ovule differentiation in WT and *osmads2 osmads4kd* double mutant.

Supplemental Figure S10. Analysis on *PI-OX* rice transgenic lines.

Supplemental Figure S11. Supporting gene expression analyses.

Supplemental Figure S12. Circular phylogenetic tree of MYB TFs from rice and MYB TFs subgroup 9A R2R3 (MIXTA) from Arabidopsis and *Phalaenopsis aphrodite*.

Supplemental Figure S13. Supporting analysis on DNA *cis* motifs in peak regions bound by OsMADS2.

Supplemental Figure S14. ChIP-qPCR validation of OsMADS2 binding to *EGL1* locus in a pool of 1-2 cm wild type inflorescences.

Supplemental Figure S15. An OsMADS2 Gene Regulatory Network constructed for gene regulation in 0.2-0.5 cm inflorescences.

Table S1: Analysis of different *osmads2* mutant alleles segregation by Chi-square test.

Table S2: Summary of genotyping and phenotyping data from the two phenotypic groups of *osmads2 osmads4kd* double mutant plants

Table S3: Sequences of the different primers and oligos used in this study

Dataset 1: ChIP-Seq peaks enriched in OsMADS2 IP

Dataset 2: List of DEGs in different *osmads2* datasets

Dataset 3: List of Gene Ontology terms enriched in different *osmads2* DEG data subsets

Dataset 4: List of DEGs in *osmads2* that have orthologs deregulated in Arabidopsis pi-1 mutant

Dataset 5: Supporting analysis of the GRNs. List of DEGs in early and middle *osmads2* expression datasets with respective occurrence number for DNA binding motifs of the different nodal transcription factors.

Acknowledgments

We acknowledge inputs from members of the UVR laboratory during the course of this study and inputs from Prof. Kalika Prasad on the manuscript draft. We acknowledge the DBT-IISc Partnership Divisional Bio-imaging and Greenhouse Facilities and thank Murthy and Jagadeesh for assistance in plant growth and care.

Funding

This study was funded by the Department of Biotechnology, Ministry of Science and Technology, Government of India, grant No. BT/PR38988/AGIII/103/1232/2020 to UVR. Project Title: Defining gene targets of rice *OsMADS2* a transcriptional regulator of floral organ differentiation and fertility**.** Research fellowships to MZ, SP and RP were recieved from the Indian Institute of Science.

References

Ahmad, I., Devonshire, J., Mohamed, R., Schultze, M., and Maathuis, F.J.M. (2016). Overexpression of the potassium channel TPKb in small vacuoles confers osmotic and drought tolerance to rice. New Phytol. **209**: 1040–1048.

Akiyama, T., Jin, S., Yoshida, M., Hoshino, T., Opassiri, R., and Ketudat Cairns, J.R. (2009). Expression of an endo-(1,3;1,4)-beta-glucanase in response to wounding, methyl jasmonate, abscisic acid and ethephon in rice seedlings. J. Plant Physiol. **166**: 1814–1825.

Ambrose, B.A., Lerner, D.R., Ciceri, P., Padilla, C.M., Yanofsky, M.F., and Schmidt, R.J. (2000). Molecular and Genetic Analyses of the Silky1 Gene Reveal Conservation in Floral Organ Specification between Eudicots and Monocots. Mol. Cell **5**: 569–579.

Balázsi, G., Van Oudenaarden, A., and Collins, J.J. (2011). Cellular decision making and biological noise: from microbes to mammals. Cell **144**: 910–925.

Bartlett, M.E., Williams, S.K., Taylor, Z., Deblasio, S., Goldshmidt, A., Hall, D.H., Schmidt, R.J., Jackson, D.P., and Whipplea, C.J. (2015). The Maize PI/GLO Ortholog Zmm16/sterile tassel silky ear1 Interacts with the Zygomorphy and Sex Determination Pathways in Flower Development. Plant Cell **27**: 3081–3098.

Bowman, J.L., Smyth, D.R., and Meyerowitz, E.M. (1989). Genes directing flower development in Arabidopsis. Plant Cell **1**: 37–52.

Busk, P.K. and Pagès, M. (1997). Microextraction of Nuclear Proteins from Single Maize Embryos. Plant Mol. Biol. Report. **15**: 371–376.

Chow, C.N., Lee, T.Y., Hung, Y.C., Li, G.Z., Tseng, K.C., Liu, Y.H., Kuo, P.L., Zheng, H.Q., and Chang, W.C. (2019). PlantPAN3.0: a new and updated resource for reconstructing transcriptional regulatory networks from ChIP-seq experiments in plants. Nucleic Acids Res. **47**: D1155–D1163.

Chung, Y.Y., Kim, S.R., Kang, H.G., Noh, Y.S., Park, M.C., Finkel, D., and An, G. (1995). Characterization of two rice MADS box genes homologous to GLOBOSA. Plant Sci. **109**: 45–56.

Coen, E.S. and Meyerowitz, E.M. (1991). The war of the whorls: genetic interactions controlling flower development. Nat. 1991 3536339 **353**: 31–37.

Cosgrove, D.J. (1999). Enzymes and other agents that enhance cell wall extensibility. Annu. Rev. Plant Physiol. Plant Mol. Biol. **50**: 391–417.**Kang, H.G., Jeon, J.S., Lee, S., and An, G.** (1998). Identification of class B and class C floral organ identity genes from rice plants. Plant Mol. Biol. **38**: 1021–1029.

Elowitz, M.B., Levine, A.J., Siggia, E.D., and Swain, P.S. (2002). Stochastic gene expression in a single cell. Science **297**: 1183–1186.

Elowitz, M.B., Levine, A.J., Siggia, E.D., and Swain, P.S. (2002). Stochastic gene expression in a single cell. Science **297**: 1183–1186.

Favaro, R., Pinyopich, A., Battaglia, R., Kooiker, M., Borghi, L., Ditta, G., Yanofsky, M.F., Kater, M.M., and Colombo, L. (2003). MADS-Box Protein Complexes Control Carpel and Ovule Development in Arabidopsis. Plant Cell **15**: 2603–2611.

Gaidatzis, D., Burger, L., Florescu, M., and Stadler, M.B. (2015). Analysis of intronic and exonic reads in RNA-seq data characterizes transcriptional and post-transcriptional regulation. Nat. Biotechnol. 2015 337 **33**: 722–729.

Gómez-Ariza, J., Brambilla, V., Vicentini, G., Landini, M., Cerise, M., Carrera, E., Shrestha, R., Chiozzotto, R., Galbiati, F., Caporali, E., López Díaz, I., and Fornara, F. (2019). A transcription factor coordinating internode elongation and photoperiodic signals in rice. Nat. Plants 2019 54 **5**: 358–362.

Gómez-Ariza, J., Brambilla, V., Vicentini, G., Landini, M., Cerise, M., Carrera, E., Shrestha, R., Chiozzotto, R., Galbiati, F., Caporali, E., López Díaz, I., and Fornara, F. (2019). A transcription factor coordinating internode elongation and photoperiodic signals in rice. Nat. Plants 2019 54 **5**: 358–362.

Hayama, R., Yokoi, S., Tamaki, S., Yano, M., and Shimamoto, K. (2003). Adaptation of photoperiodic control pathways produces short-day flowering in rice. Nat. 2003 4226933 **422**: 719–722.

Heslop-Harrison, Y. and Heslop-Harrison, J.S. (1996). Lodicule Function and Filament Extension in the Grasses: Potassium Ion Movement and Tissue Specialization. Ann. Bot. **77**: 573–582.

Hill, T.A., Day, C.D., Zondlo, S.C., Thackeray, A.G., and Irish, V.F. (1998). Discrete spatial and temporal cis-acting elements regulate transcription of the Arabidopsis floral homeotic gene APETALA3. Development **125**: 1711–1721.

Hong, L., Tang, D., Zhu, K., Wang, K., Li, M., and Cheng, Z. (2012). Somatic and Reproductive Cell Development in Rice Anther Is Regulated by a Putative Glutaredoxin. Plant Cell **24**: 577–588.

Hongo, S., Sato, K., Yokoyama, R., and Nishitani, K. (2012). Demethylesterification of the primary wall by PECTIN METHYLESTERASE35 provides mechanical support to the Arabidopsis stem. Plant Cell **24**: 2624–2634.

Honma, Y. et al. (2020). High-quality sugar production by osgcs1 rice. Commun. Biol. 2020 31 **3**: 1–8.

Hu, Y. et al. (2021). Rice transcription factor MADS32 regulates floral patterning through interactions with multiple floral homeotic genes. J. Exp. Bot. **72**: 2434–2449.

Irish, V.F. (2010). The flowering of Arabidopsis flower development. Plant J. **61**: 1014–1028.

Itoh, J.-I., Nonomura, K.-I., Ikeda, K., Yamaki, S., Inukai, Y., Yamagishi, H., Kitano, H., and Nagato, Y. (2005). Rice Plant Development: from Zygote to Spikelet. Plant Cell Physiol **46**: 23–47.

Jack, T., Fox, G.L., and Meyerowitz, E.M. (1994). Arabidopsis homeotic gene APETALA3 ectopic expression: transcriptional and posttranscriptional regulation determine floral organ identity. Cell **76**: 703–716.

Jackson, A.L., Bartz, S.R., Schelter, J., Kobayashi, S. V., Burchard, J., Mao, M., Li, B., Cavet, G., and Linsley, P.S. (2003). Expression profiling reveals off-target gene regulation by RNAi. Nat. Biotechnol. **21**: 635–637.

Jang, S. and Li, H.Y. (2017). Oryza sativa BRASSINOSTEROID UPREGULATED1 LIKE1 induces the expression of a gene encoding a small leucine-rich-repeat protein to positively regulate lamina inclination and grain size in rice. Front. Plant Sci. **8**: 1253.

Ji, J. and Braam, J. (2010). Restriction Site Extension PCR: A Novel Method for High-Throughput Characterization of Tagged DNA Fragments and Genome Walking. PLoS One **5**: e10577.

Jin, Y. et al. (2011). An AT-hook gene is required for palea formation and floral organ number control in rice. Dev. Biol. **359**: 277–288.

Joldersma, D. and Liu, Z. (2018). The making of virgin fruit: the molecular and genetic basis of parthenocarpy. J. Exp. Bot. **69**: 955–962.

Kang, H.G., Jeon, J.S., Lee, S., and An, G. (1998). Identification of class B and class C floral organ identity genes from rice plants. Plant Mol. Biol. **38**: 1021–1029.

Kong, L., Duan, Y., Ye, Y., Cai, Z., Wang, F., Qu, X., Qiu, R., Wu, C., and Wu, W. (2019). Screening and analysis of proteins interacting with OsMADS16 in rice (Oryza sativa L.). PLoS One **14**: e0221473.

Kouzai, Y., Nakajima, K., Hayafune, M., Ozawa, K., Kaku, H., Shibuya, N., Minami, E., and Nishizawa, Y. (2014). CEBiP is the major chitin oligomer-binding protein in rice and plays a main role in the perception of chitin oligomers. Plant Mol. Biol. **84**: 519–528.

Krizek, B.A. and Fletcher, J.C. (2005). Molecular mechanisms of flower development: an armchair guide. Nat. Rev. Genet. 2005 69 **6**: 688–698.

Krizek, B.A. and Meyerowitz, E.M. (1996). The Arabidopsis homeotic genes APETALA3 and PISTILLATA are sufficient to provide the B class organ identity function. Development **122**: 11–22.

Krizek, B.A. and Meyerowitz, E.M. (1996). The Arabidopsis homeotic genes APETALA3 and PISTILLATA are sufficient to provide the B class organ identity function. Development **122**: 11–22.

Krizek, B.A. and Meyerowitz, E.M. (1996). The Arabidopsis homeotic genes APETALA3 and PISTILLATA are sufficient to provide the B class organ identity function. Development **122**: 11–22.

Kyozuka, J., Kobayashi, T., Morita, M., and Shimamoto, K. (2000). Spatially and temporally regulated expression of rice MADS box genes with similarity to Arabidopsis class A, B and C genes. Plant Cell Physiol. **41**: 710–718.

Lee, J.H., Park, S.H., and Ahn, J.H. (2012). Functional conservation and diversification between rice OsMADS22/OsMADS55 and Arabidopsis SVP proteins. Plant Sci. **185**–**186**: 97–104.

Lee, S., Jeon, J.S., An, K., Moon, Y.H., Lee, S., Chung, Y.Y., and An, G. (2003). Alteration of floral organ identity in rice through ectopic expression of OsMADS16. Planta **217**: 904–911.

Li, N. et al. (2006). The rice tapetum degeneration retardation gene is required for tapetum degradation and anther development. Plant Cell **18**: 2999–3014.

Li, Q., Tong, T., Jiang, W., Cheng, J., Deng, F., Wu, X., Chen, Z.H., Ouyang, Y., and Zeng, F. (2022). Highly Conserved Evolution of Aquaporin PIPs and TIPs Confers Their Crucial Contribution to Flowering Process in Plants. Front. Plant Sci. **12**: 2945.

Li, Y., Ouyang, J., Wang, Y.Y., Hu, R., Xia, K., Duan, J., Wang, Y., Tsay, Y.F., and Zhang, M. (2015). Disruption of the rice nitrate transporter OsNPF2.2 hinders root-to-shoot nitrate transport and vascular development. Sci. Reports 2015 51 **5**: 1–10.

Lohmann, J.U. and Weigel, D. (2002). Building beauty: the genetic control of floral patterning. Dev. Cell **2**: 135–142.

Lu, H.C., Lam, S.H., Zhang, D., Hsiao, Y.Y., Li, B.J., Niu, S.C., Li, C.Y., Lan, S., Tsai, W.C., and Liu, Z.J. (2022). R2R3-MYB genes coordinate conical cell development and cuticular wax biosynthesis in Phalaenopsis aphrodite. Plant Physiol. **188**: 318–331.

Luan, X., Liu, S., Ke, S., Dai, H., Xie, X.M., Hsieh, T.F., and Zhang, X.Q. (2019). Epigenetic modification of ESP, encoding a putative long noncoding RNA, affects panicle architecture in rice. Rice **12**.

Machanick, P. and Bailey, T.L. (2011). MEME-ChIP: motif analysis of large DNA datasets. Bioinformatics **27**: 1696–1697.

Nagasawa, N., Miyoshi, M., Sano, Y., Satoh, H., Hirano, H., Sakai, H., and Nagato, Y. (2003). SUPERWOMAN1 and DROOPING LEAF genes control floral organ identity in rice. Development **130**: 705–718.

Nakagawa, M., Shimamoto, K., and Kyozuka, J. (2002). Overexpression of RCN1 and RCN2, rice TERMINAL FLOWER 1/CENTRORADIALIS homologs, confers delay of phase transition and altered panicle morphology in rice. Plant J. **29**: 743–750.

Ning, J., Zhang, B., Wang, N., Zhou, Y., and Xiong, L. (2011). Increased Leaf Angle1, a Raf-Like MAPKKK That Interacts with a Nuclear Protein Family, Regulates Mechanical Tissue Formation in the Lamina Joint of Rice. Plant Cell **23**: 4334–4347.

Pagès, H., Aboyoun, P., Gentleman, R. and DebRoy, S. (2022). *Biostrings: Efficient manipulation of biological strings*. R package version 2.64.0, https://bioconductor.org/packages/Biostrings.

Pinyopich, A., Ditta, G.S., Savidge, B., Liljegren, S.J., Baumann, E., Wisman, E., and Yanofsky, M.F. (2003). Assessing the redundancy of MADS-box genes during carpel and ovule development. Nature **424**: 85–88.

Prasad, K. and Vijayraghavan, U. (2003). Double-stranded RNA interference of a rice PI/GLO paralog, OsMADS2, uncovers its second-whorl-specific function in floral organ patterning. Genetics **165**: 2301–2305.

Reed, A., Rudall, P.J., Brockington, S.F., Glover, B.J., and Bartlett, M. (2022). Conical petal epidermal cells, regulated by the MYB transcription factor MIXTA, have an ancient origin within the angiosperms. J. Exp. Bot. **73**: 5490–5502.

Ren, L., Tang, D., Zhao, T., Zhang, F., Liu, C., Xue, Z., Shi, W., Du, G., Shen, Y., Li, Y., and Cheng, Z. (2018). OsSPL regulates meiotic fate acquisition in rice. New Phytol. **218**: 789–803.

Sakurai, J., Ishikawa, F., Yamaguchi, T., Uemura, M., and Maeshima, M. (2005). Identification of 33 Rice Aquaporin Genes and Analysis of Their Expression and Function. Plant Cell Physiol. **46**: 1568–1577.

Sato, Y., Takehisa, H., Kamatsuki, K., Minami, H., Namiki, N., Ikawa, H., Ohyanagi, H., Sugimoto, K., Antonio, B.A., and Nagamura, Y. (2013). RiceXPro Version 3.0: expanding the informatics resource for rice transcriptome. Nucleic Acids Res. **41**: D1206–D1213.

Scarpella, E., Rueb, S., Boot, K.J.M., Hoge, J.H.C., and Meijer, A.H. (2000). A role for the rice homeobox gene Oshox1 in provascular cell fate commitment. Development **127**: 3655–3669.

Schmidt, R., Schippers, J.H.M., Welker, A., Mieulet, D., Guiderdoni, E., and Mueller-Roeber, B. (2012). Transcription factor OsHsfC1b regulates salt tolerance and development in Oryza sativa ssp. japonica. AoB Plants **2012**.

Schwarz-Sommer, Z., Huijser, P., Nacken, W., Saedler, H., and Sommer, H. (1990). Genetic Control of Flower Development by Homeotic Genes in Antirrhinum majus. Science **250**: 931–936.

Suzaki, T., Sato, M., Ashikari, M., Miyoshi, M., Nagato, Y., and Hirano, H.Y. (2004). The gene FLORAL ORGAN NUMBER1 regulates floral meristem size in rice and encodes a

leucine-rich repeat receptor kinase orthologous to Arabidopsis CLAVATA1. Development **131**: 5649–5657.

Tan, H., Liang, W., Hu, J., and Zhang, D. (2012). MTR1 encodes a secretory fasciclin glycoprotein required for male reproductive development in rice. Dev. Cell **22**: 1127–1137.

Uchiumi, T. and Okamoto, T. (2010). Rice fruit development is associated with an increased IAA content in pollinated ovaries. Planta **232**: 579–592.

Uji, Y., Kashihara, K., Kiyama, H., Mochizuki, S., Akimitsu, K., and Gomi, K. (2019). Jasmonic Acid-Induced VQ-Motif-Containing Protein OsVQ13 Influences the OsWRKY45 Signaling Pathway and Grain Size by Associating with OsMPK6 in Rice. Int. J. Mol. Sci. **20**.

Veronico, P., Rosso, L.C., Melillo, M.T., Fanelli, E., De Luca, F., Ciancio, A., Colagiero, M., and Pentimone, I. (2022). Water Stress Differentially Modulates the Expression of Tomato Cell Wall Metabolism-Related Genes in Meloidogyne incognita Feeding Sites. Front. Plant Sci. **13**: 776.

Wang, M. et al. (2022). Methylesterification of cell-wall pectin controls the diurnal flower-opening times in rice. Mol. Plant **15**: 956–972.

Wang, H., Zhang, L., Cai, Q., Hu, Y., Jin, Z., Zhao, X., Fan, W., Huang, Q., Luo, Z., Chen, M., Zhang, D., and Yuan, Z. (2015). OsMADS32 interacts with PI-like proteins and regulates rice flower development. J. Integr. Plant Biol. **57**: 504–513.

Wang, S., Wu, K., Yuan, Q., Liu, X., Liu, Z., Lin, X., Zeng, R., Zhu, H., Dong, G., Qian, Q., Zhang, G., and Fu, X. (2012). Control of grain size, shape and quality by OsSPL16 in rice. Nat. Genet. 2012 448 **44**: 950–954.

Wang, Y., Chantreau, M., Sibout, R., and Hawkins, S. (2013). Plant cell wall lignification and monolignol metabolism. Front. Plant Sci. **4**.

Whipple, C.J., Ciceri, P., Padilla, C.M., Ambrose, B.A., Bandong, S.L., and Schmidt, R.J. (2004). Conservation of B-class floral homeotic gene function between maize and Arabidopsis. Development **131**: 6083–6091.

Winter, C.M. et al. (2011). LEAFY Target Genes Reveal Floral Regulatory Logic, cis Motifs, and a Link to Biotic Stimulus Response. Dev. Cell **20**: 430–443.

Wu, W., Zhang, Y., Zhang, M., Zhan, X., Shen, X., Yu, P., Chen, D., Liu, Q., Sinumporn, S., Hussain, K., Cheng, S., and Cao, L. (2018). The rice CONSTANS-like protein OsCOL15 suppresses flowering by promoting Ghd7 and repressing RID1. Biochem. Biophys. Res. Commun. **495**: 1349–1355.

Wuest, S.E., O'Maoileidigh, D.S., Rae, L., Kwasniewska, K., Raganelli, A., Hanczaryk, K., Lohan, A.J., Loftus, B., Graciet, E., and Wellmer, F. (2012). Molecular basis for the specification of floral organs by APETALA3 and PISTILLATA. Proc. Natl. Acad. Sci. U. S. A. **109**: 13452–13457.

Xie, G., Yang, B., Xu, Z., Li, F., Guo, K., Zhang, M., Wang, L., Zou, W., Wang, Y., and Peng, L. (2013). Global Identification of Multiple OsGH9 Family Members and Their Involvement in Cellulose Crystallinity Modification in Rice. PLoS One **8**: e50171.

Xu, P. et al. (2022). EARLY MORNING FLOWERING1 (EMF1) regulates the floret opening time by mediating lodicule cell wall formation in rice. Plant Biotechnol. J. **20**: 1441–1443.

Xu, Q., Yu, X., Cui, Y., Xia, S., Zeng, D., Qian, Q., and Ren, D. (2020). LRG1 maintains sterile lemma identity by regulating OsMADS6 expression in rice. Sci. China Life Sci. 2020 647 **64**: 1190–1192.

Yadav, S.R., Prasad, K., and Vijayraghavan, U. (2007). Divergent regulatory OsMADS2 functions control size, shape and differentiation of the highly derived rice floret second-whorl organ. Genetics **176**: 283–294.

Yang, Y., Xiang, H., and Jack, T. (2003). pistillata-5, an Arabidopsis B class mutant with strong defects in petal but not in stamen development. Plant J. **33**: 177–188.

Yao, S.G., Ohmori, S., Kimizu, M., and Yoshida, H. (2008). Unequal Genetic Redundancy of Rice PISTILLATA Orthologs, OsMADS2 and OsMADS4, in Lodicule and Stamen Development. Plant Cell Physiol. **49**: 853–857.

Yao, S.G., Ohmori, S., Kimizu, M., and Yoshida, H. (2008). Unequal Genetic Redundancy of Rice PISTILLATA Orthologs, OsMADS2 and OsMADS4, in Lodicule and Stamen Development. Plant Cell Physiol. **49**: 853–857.

Yoshida, A., Suzaki, T., Tanaka, W., and Hirano, H.Y. (2009). The homeotic gene long sterile lemma (G1) specifies sterile lemma identity in the rice spikelet. Proc. Natl. Acad. Sci. U. S. A. **106**: 20103–20108.

Yoshida, H., Itoh, J.I., Ohmori, S., Miyoshi, K., Horigome, A., Uchida, E., Kimizu, M., Matsumura, Y., Kusaba, M., Satoh, H., and Nagato, Y. (2007). superwoman1-cleistogamy, a hopeful allele for gene containment in GM rice. Plant Biotechnol. J. **5**: 835–846.

Yu, G., Wang, L.G., and He, Q.Y. (2015). ChIPseeker: an R/Bioconductor package for ChIP peak annotation, comparison and visualization. Bioinformatics **31**: 2382–2383.

Yun, D., Liang, W., Dreni, L., Yin, C., Zhou, Z., Kater, M.M., and Zhang, D. (2013). OsMADS16 genetically interacts with OsMADS3 and OsMADS58 in specifying. Mol. Plant **6**: 743–756.

Zeng, Y.X., Hu, C.Y., Lu, Y.G., Li, J.Q., and Liu, X.D. (2007). Diversity of abnormal embryo sacs in indica/japonica hybrids in rice demonstrated by confocal microscopy of ovaries. Plant Breed. **126**: 574–580.

Zhang, Y., Liu, T., Meyer, C.A., Eeckhoute, J., Johnson, D.S., Bernstein, B.E., Nussbaum, C., Myers, R.M., Brown, M., Li, W., and Shirley, X.S. (2008). Model-based analysis of ChIP-Seq (MACS). Genome Biol. **9**: 1–9.

Zhang, D., Luo, X., and Zhu, L. (2011). Cytological analysis and genetic control of rice anther development. J. Genet. Genomics **38**: 379–390.

Zhang, H., Liang, W., Yang, X., Luo, X., Jiang, N., Ma, H., and Zhang, D. (2010). Carbon Starved Anther Encodes a MYB Domain Protein That Regulates Sugar Partitioning Required for Rice Pollen Development. Plant Cell **22**: 672–689.

Zhao, Z. et al. (2013). A Role for a Dioxygenase in Auxin Metabolism and Reproductive Development in Rice. Dev. Cell **27**: 113–122.

Zhu, L.J., Gazin, C., Lawson, N.D., Pagès, H., Lin, S.M., Lapointe, D.S., and Green, M.R. (2010). ChIPpeakAnno: A Bioconductor package to annotate ChIP-seq and ChIP-chip data. BMC Bioinformatics **11**: 1–10.

Zik, M. and Irish, V.F. (2003). Global identification of target genes regulated by APETALA3 and PISTILLATA floral homeotic gene action. Plant Cell **15**: 207–222.

Zong, J. et al. (2022). A rice single cell transcriptomic atlas defines the developmental trajectories of rice floret and inflorescence meristems. New Phytol. **234**: 494–512.

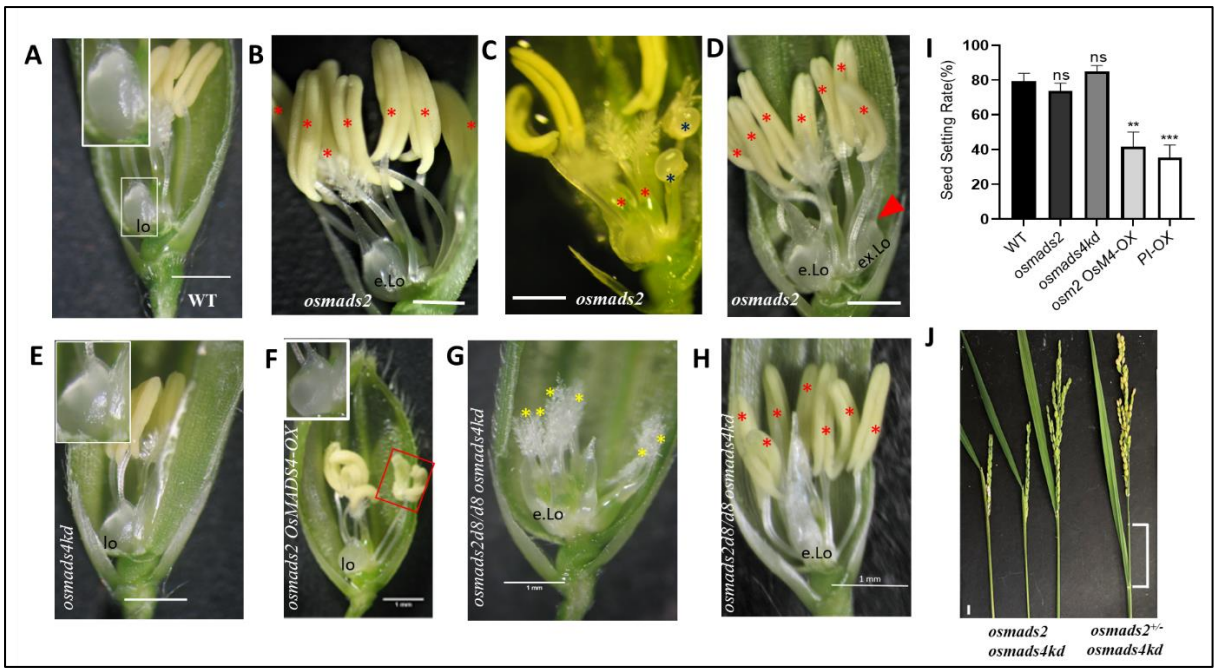

Figure 1. Phenotypic analysis of the different genotypes studied. A, WT mature pre-anthesis spikelet dissected to show the lodicule. The inset shows a magnification of the normal lodicule. B-D, *osmads2* mutant spikelets dissected to show abnormal organs. In B and D, the red asterisks mark the increased stamen number. In D, the red arrowhead marks the extra lodicule (ex.Lo). In C, two red asterisks mark ectopic carpels and the fourth whorl carpel. The dark blue asterisks mark the stamen-carpel chimeric organs in this *osmads2* mutant spikelet that resemble partially *spw*-like. E, Spikelet dissected from *osmads4kd#1* showing apparently normal internal floral organs. F, Spikelet from *osmads2 OsMADS4-OX* line #3 showing apparently normal lodicule in the complemented line with abnormal crescent-like anthers (red rectangle). G and H, Spikelets from *osmads2d8/d8 osmads4kd* of representative group I and group II phenotypes, respectively. The yellow asterisks represent the main and ectopic carpels in group I phenotype and the red asterisks mark the increased stamen number in group II phenotype. The elongated lodicule (e.Lo) is flattened throughout the proximal distal axis (compare lodicule in G and H *vs* in A and B). I, Plot graph depicting the seed setting rate in the different generated genotypes studied. Statistical t test was employed. Double asterisks and triple asterisks indicate P value < 0.01 and < 0.001, respectively. The error bars represent the SEM. J, Panicle partially enclosure phenotype in flag leaf sheath in *osmads2d8/d8 osmads4kd* plants. Scale bars: 1 mm in A-H, 1 cm in J.

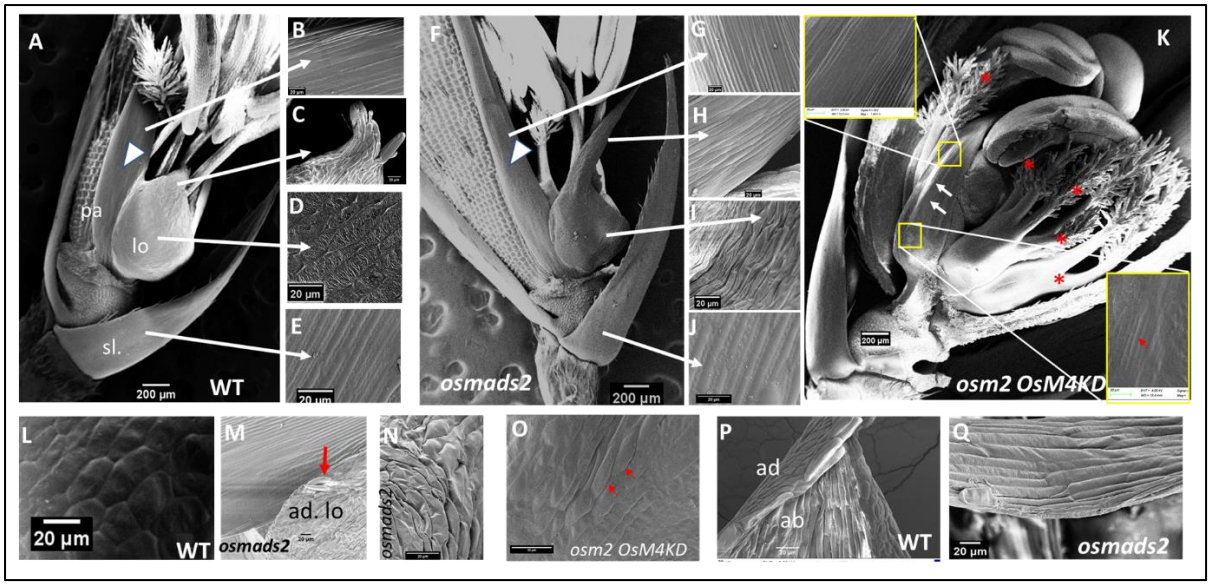

Figure 2. Comparison of epidermal morphologies in floral whorl organs of wild-type *vs*. *osmads2*$^{d8/d8}$ mutant *vs. osmads2*$^{d8/d8}$ *osmads4kd* by SEM. A, F and K, Partially dissected florets where the lemma has been removed. Open arrowhead points to the palea marginal tissue in A and in higher magnification in B. C, D, and E, Abaxial cells from WT apical/distal lodicule, basal/proximal lodicule, and sterile lemma, respectively. G, H, I, and J, Abaxial epidermal surfaces of *osmads2* mutant marginal tissue of palea, apical/distal lodicule, basal/proximal lodicule, and sterile lemma, respectively. The elongated cells of the epidermal layer of the mutant lodicule phenocopy the cells of the epidermal layers in mtp (Compare C and D *vs* H and I *vs* insets in K). In K, the white arrows point to the abnormally developed midrib in the transformed lodicule. The red asterisks indicate the ectopic carpels and the red arrow shows the elongated cells in the epidermal surface of the lodicule. L, Abaxial cell surface of the basal/proximal portion of WT lodicule. M, Adaxial surface of *osmads2* lodicule with trichomes (red arrow). N and O, Abaxial surface of the basal/proximal portion of *osmads2* lodicule and *osmads2 osmads4kd* lodicule, respectively. Comparison of N and O to L shows that mutant lodicules have abnormally elongated epidermal cells (red arrows). P and Q, Adaxial surfaces of distal portion of lodicules showing cell elongation in *osmads2* (Q) as compared to WT (P). pa, lo, sl, ad, and ab stand for palea, lodicule, sterile lemma, adaxial and abaxial, respectively.

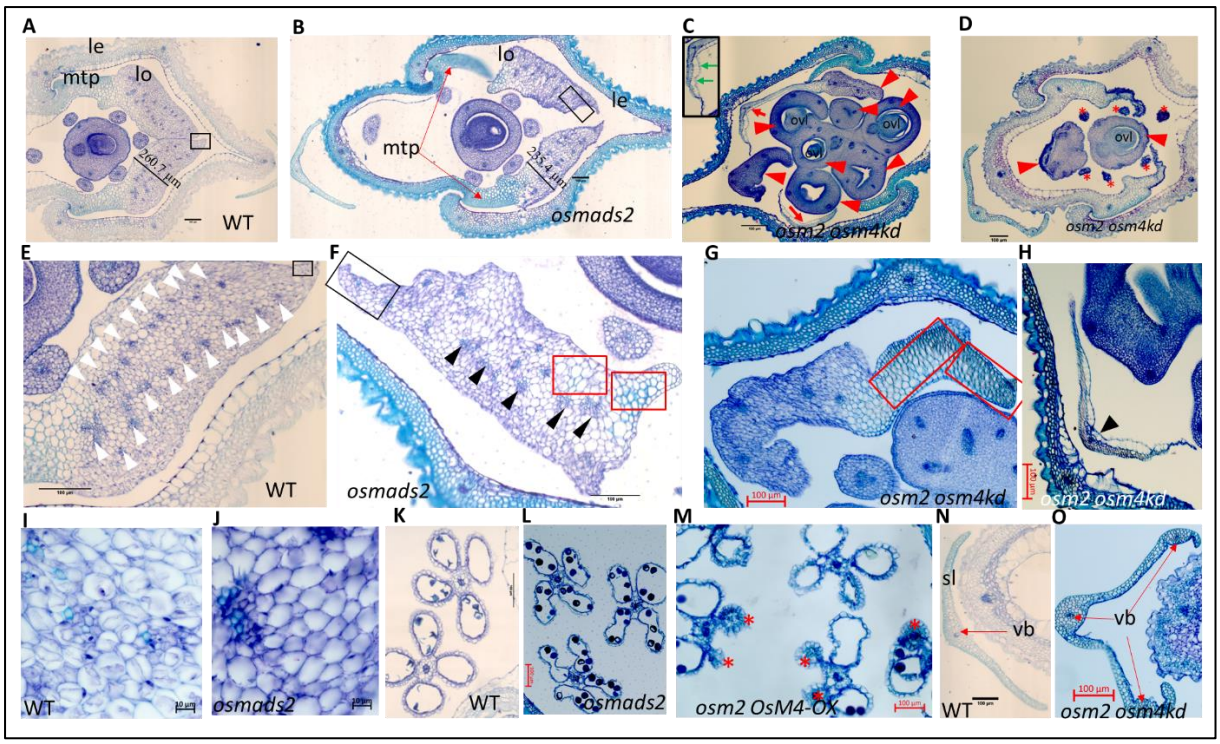

Figure 3. Histological transverse sections (TS) of spikelets reveal cell proliferation and differentiation defects in florets of different genotypes. A and B, TS at the basal region of WT and *osmads2*$^{d8/d8}$ florets, respectively. The black box marks the peripheral regions of the lodicule that underlie the lemma which are overgrown in the transformed lodicules as compared to WT lodicules. The black lines mark the width of the lodicule across the abaxial-adaxial axis. C; TS in double mutant *osmads2*$^{d8/d8}$ *osmads4kd* spikelet with phenotype group I. Red arrows point to the midvein in the abnormal lodicule. The lodicule is stained green as for organs with lignified cell walls. The inset shows that the adaxial side of the abnormal lodicule is lined with bubble-shaped cells resembling those lining the lemma and palea. D, TS of double mutant *osmads2*$^{d8/d8}$ *osmads4kd* spikelet with group II phenotype. The internal floral organ number is increased in C and D. The stamens in D are indicated by asterisk and the red arrowheads in C and D point towards the central and ectopic carpels. The abnormal lodicule is stained green as of the mtp. The sterile lemma is abnormal. E-H**,** TS sections of lodicules in WT and *osmads2*$^{d8/d8}$, *osmads2*$^{d8/d8}$ *osmads4kd* group I and group II, respectively. The red rectangles (in F and G) mark green stained regions which indicate cell wall lignification. The black arrowheads mark the vascular bundles which are reduced in number and of abnormal distribution across the lodicule of *osmads2*$^{d8/d8}$. I and J, TS of lodicules in WT and *osmads2*$^{d8/d8}$ at high magnification (40X) showing the cell shape in ground tissues. Compare the brick-like parenchyma (I) to the polygonal like cells in J. K-M, TS of anthers from WT, *osmads2*$^{d8/d8}$ and *osmads2 OsMADS4-OX* florets, respectively. The anther sections in *osmads2 OsMADS4-OX* show defective stamen; the red asterisks pointing at underdeveloped locules. N and O, Sections of the sterile lemma. The sterile lemma in *osmads2*$^{d8/d8}$ *osmads4kd* florets (O) is abnormal as compared to WT (N). Abbreviation: le; lemma, pa; palea, lo; lodicule, mtp; marginal tissue of palea, vp; vascular bundles, gl; glumes, ovl; ovule-like

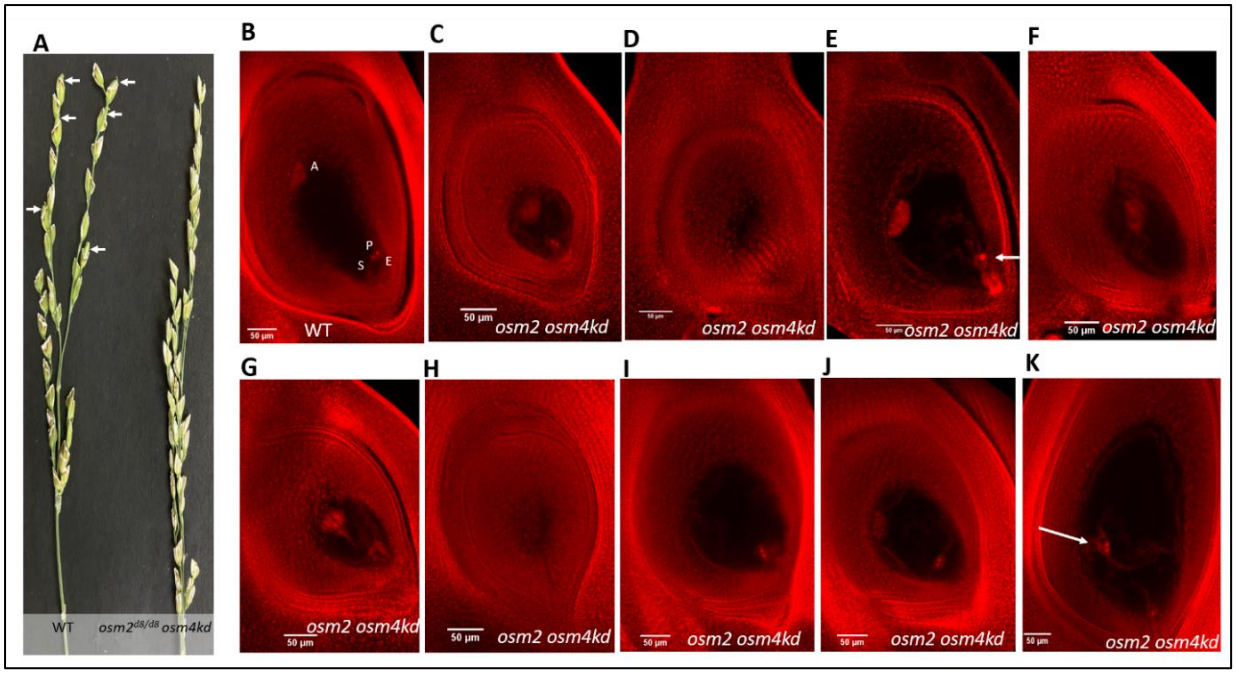

Figure 4. Female sterility in *osmads2 osmads4kd* double mutants. A, Emasculated WT and *osmads2 osmads4kd* double mutant inflorescences dusted with pollens from WT, show development of seed (white arrows) in WT but not in *osmads2 osmads4kd* (*osm2 osm4kd*) double mutant. B-K, Ovaries and ovules from pre-anthesis WT and *osmads2 osmads4kd* florets. B, Ovule of WT with normal embryo sac constituting A; antipodal cells, P; polar nuclei, E; egg cell, S; Synergid cells. C, Ovule from *osmads2 osmads4kd* floret in C has apparently normal embryo sac though smaller. D and H, Ovules with degenerated embryo sac (mass of stained cells, no full cavity). E, Embryo sac with single polar nuclei (white arrow). F, Embryo sac with no female unit, i.e., egg cells, polar nuclei and synergids. G, Embryo sac with no polar nuclei. I, Embryo sac without antipodal cells. J, Embryo sac with no egg unit (no egg, no synergids). K, Embryo sac with no antipodal cells and with mislocated polar nuclei (white arrow).

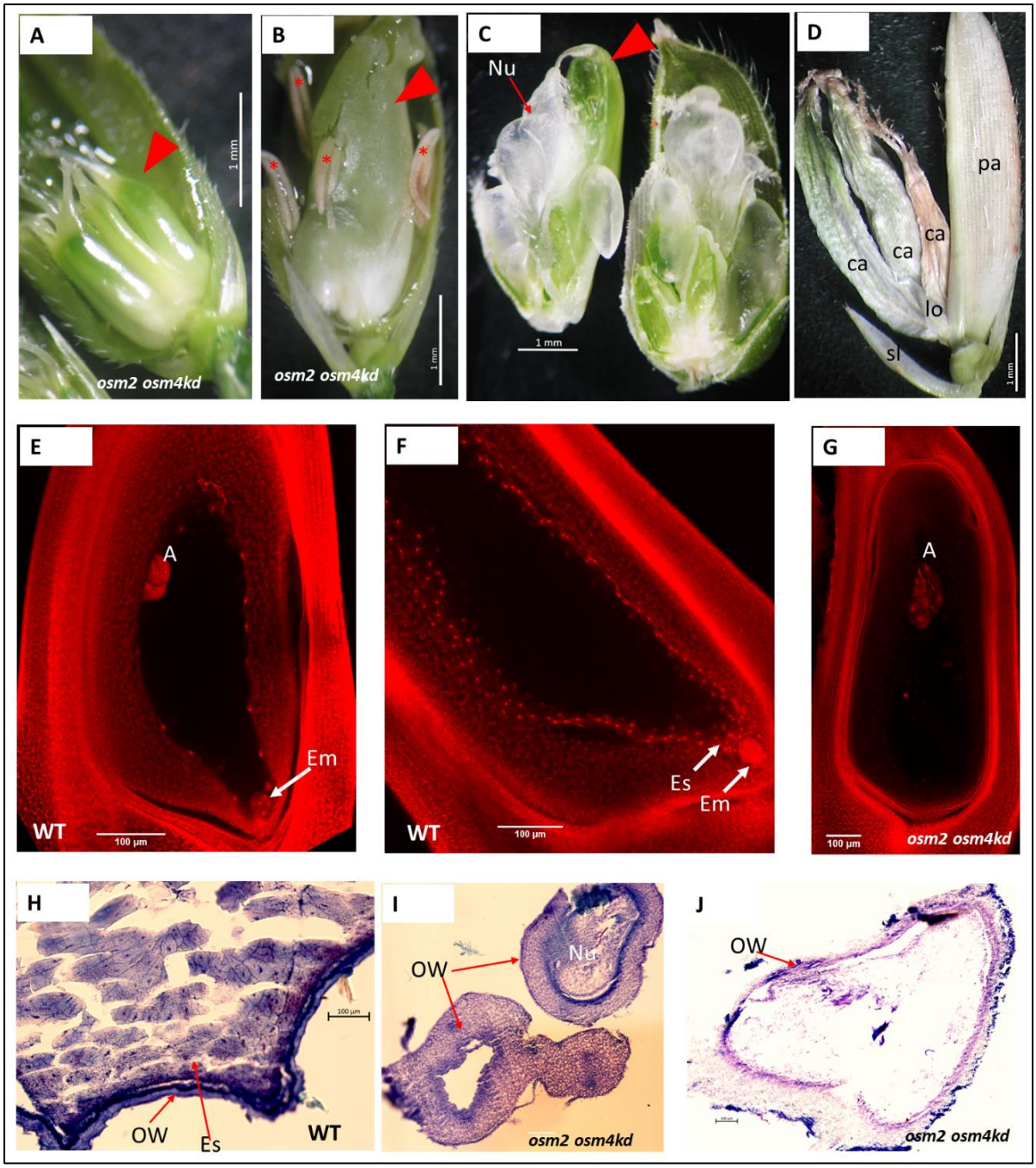

Figure 5. Parthenocarpy-like phenotypes in *osmads2$^{d8/d8}$ osmads4kd* double mutant. A and B, Pericarpic growth in double mutant florets of type I and type II phenotypes, respectively. The red arrowhead points at the expanded pericarp. In B, asterisks mark the indehiscenced empty sterile anthers. The filaments of these sterile anthers failed to extend within the unopened florets. C, Floret of *osmads2$^{d8/d8}$ osmads4kd* double mutant with pericarpic growth. The growing ovary (red arrowhead) was manually dissected to show the growing nucellar mass inside (red arrow). D, Dry spikelet from *osmads2$^{d8/d8}$ osmads4kd* double mutant where lemma is removed to show the expanded pericarps that are shrunken and dry. E-G, Confocal microscopy Z-stacked images of ovaries from WT (E and F) and *osmads2 osmads4kd* double mutant (G). The double mutant ovary lacks embryo (Em) and endosperm (Es). H and I, Transverse section of WT and double mutant pericarps, respectively. J, longitudinal section of

double mutant expanded pericarp. Unlike WT, the double mutant pericarp lacks granular endosperm. Abbreviation: Carpel (ca), lodicule (lo), palea (pl), sterile lemma (sl), ovary wall (OW).

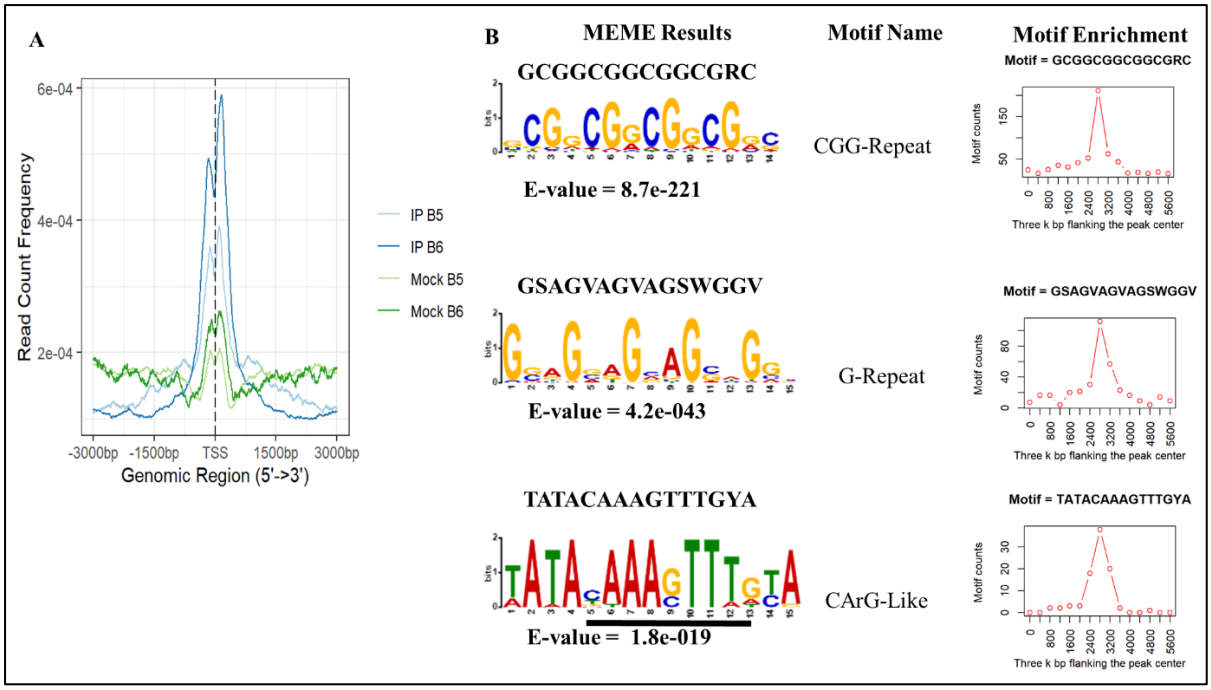

Figure 6: Analysis of genome-wide binding sites of OsMADS2 in WT panicles with developing florets. A, The plot shows relative distribution of OsMADS2 binding sites (ChIP-Seq peaks) mapped relative to TSS (from 3,000 bp upstream to 3,000 bp downstream). The blue lines represent peaks called by MACS2 algorithm using IP data over mock data. The green lines represent peaks called by MACS2 algorithm using Mock data over IP data. The Peaks of the IP over Mock show enrichment around the TSS. B, Left panel series is a representation of significantly enrich motifs in the peak regions in the global data (MEME analysis) and the right panel series shows the relative distribution of these enriched motifs around the global peak midpoints (from 3,000 bp upstream to 3,000 bp downstream of the peak midpoints).

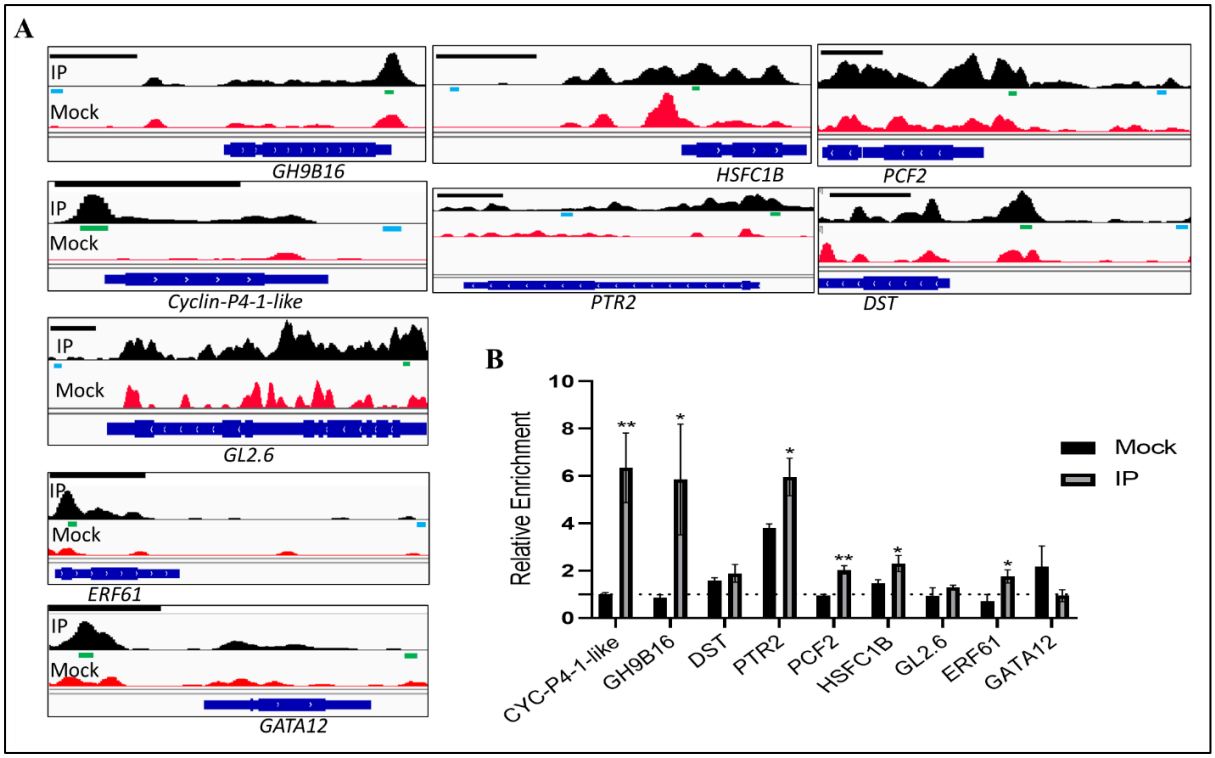

Figure 7. **ChIP-qPCR based validation of some genomic loci bound by OsMADS2 in a pool of 0.5-1 cm inflorescences with developing florets.** A, Snapshot of IGV for each locus is shown where the ChIP-Seq peak regions and nonpeak regions (Control) are represented with green and cyan lines, respectively. The black line above each IGV tab is 1kb of the genome. B, Plot representing the relative enrichment in IP and in mock, calculated as described in materials and methods after normalizing %input of the peak region PCR to the %input of nonpeak control region PCR. The dotted line represents a threshold of 1 on the y-axis which corresponds to the %input values of the nonpeak control region PCR after being divided by themselves. To test significance of enrichment in IP over mock, t test was employed. Single asterisk and double asterisk indicate pvalue ≤ 0.05 and ≤ 0.01, respectively.

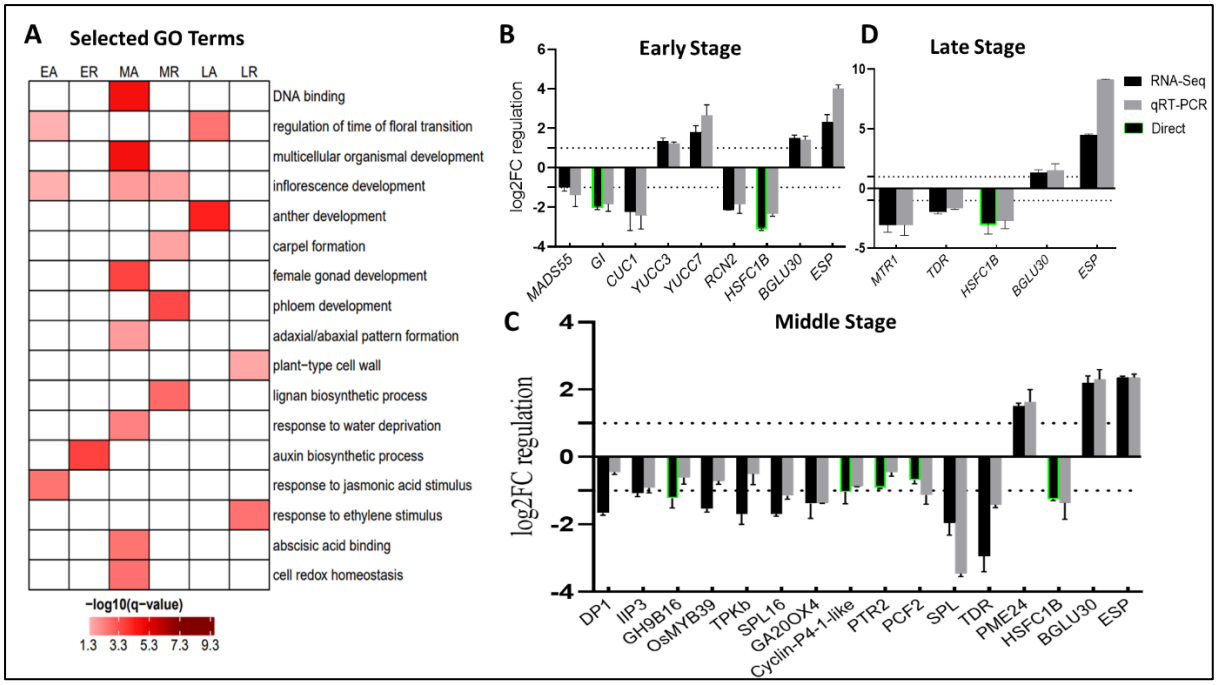

Figure 8. Gene ontology enrichment analysis and validation of RNA-Seq data. A, Heatmap representation of selected enriched GO terms in the differentially expressed gene sets. Oryzabase database (https://shigen.nig.ac.jp/rice/oryzabase/) GO annotation was used for this analysis and the significant enriched GO terms were retrieved at qvalue ≤ 0.05. B-D, Plot representations of selected genes that are differentially expressed in panicles of early (0.2-0.5 cm), middle (0.5-1 cm) and late (1-2 cm) stages. The log2FoldChange of RNA-seq data (solid black bars) was calculated from the normalized TMM expression values. Bars with green outline represent those genes that are also direct downstream targets. Those genes are deregulated as per RNA-seq and qPCR data and bound by OsMADS2 as per ChIP-Seq analysis. Error bars represent the SEM.

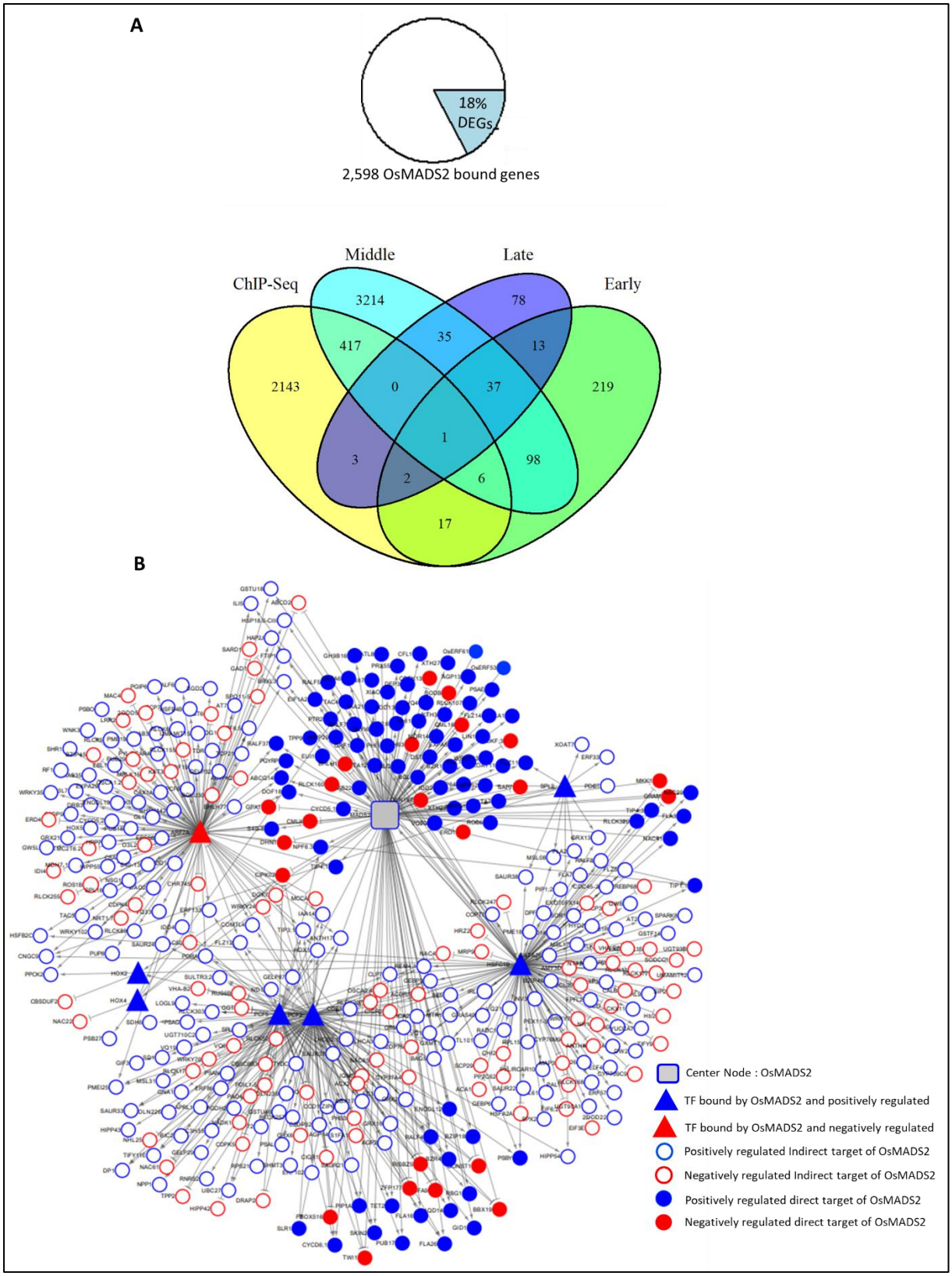

Figure 9. Analysis of gene regulatory network downstream of OsMADS2. A, Numerical representation of *OsMADS2* directly and indirectly regulated genes. The pie chart shows portion of DEGs among all OsMADS2 bound annotated loci and the Venn diagram shows overlap between the different RNA-Seq datasets and ChIP-Seq. B, Predicted OsMADS2 Gene

Regulatory Network in panicle tissues pooled for 0.5-1 cm stage which constitutes florets with differentiating organs. The blue filled nodes represents OsMADS2 direct downstream targets. The blue and red colors of the node boundaries represent positive and negative regulation by OsMADS2, respectively. The arrow shape and the T-shape indicate positive and negative regulation of the nodal gene, respectively. Filled tringles are transcription factors targets of *OsMADS2* which were used to construct the second layer in the gene regulatory network. Only genes with annotated functions and assigned gene symbols are presented in this predicted gene regulatory network. Complete list of genes predicted to be regulated (based on presence of DNA binding motif in the assumed promotor region of genes in layer 2) by the nodal transcription factors is provided in dataset 5.